ELECTROGASTROGRAPHY

ELECTROGASTROGRAPHY

By

CRAIG DEGRUCHY, B. ENG. (McMaster University)

A Thesis

Submitted to the School of Graduate Studies

in Partial Fulfillment of the Requirements

for the Degree

Master of Engineering

McMaster University

Jennifer Lonce MacAloney, whom I love with all my heart, will you marry me?

MASTER OF ENGINEERING
(Electrical & Computer Engineering)

McMaster University
Hamilton, Ontario

TITLE: **Electrogastrography**

AUTHOR: Craig DeGruchy, B. Eng. (McMaster University)

SUPERVISOR: Dr. H. deBruin

NUMBER OF PAGES: xiv , 114

ABSTRACT

Electrical activity of the stomach is one determining factor of gastric motility by controlling and coordinating contractions of the gastric musculature. These contractions, both tonic and phasic, are responsible for the storing, mixing, and emptying of food. Gastric electrical activity is therefore a very important factor for normal stomach function.

The development of a multi-channel, bandlimited, signal amplifier and recording system, provides a means to record this electrical activity. Many practical issues are addressed to provide a signal of acceptable quality and several basic signal processing techniques are applied to increase the quality of these signals and provide extraction of important information regarding power and frequency content.

Gastric electrical activity is recorded from the stomachs of several rats in various experiments. The recorded activity in different regions of the stomach, responsible for different functions, is compared and evaluated with respect to known cellular events. By introducing several stimuli and observing changes in recorded activity, the nervous control of the stomach via mediation of the electrical activity is also examined and modeled briefly.

ACKNOWLEDGEMENTS

There are many people who helped to make this research possible. I express sincere gratitude to Dr. H. de Bruin, who as been a true mentor, providing encouragement, advice and support for the past two years. The support of Dr. G. Tougas, provision of laboratory space and supplies, ideas and kind words of motivation, is also greatly appreciated. I am also indebted to Dr. L. Wang, for assistance and training in experimental methods, without whom this thesis would not have been possible. I would also like to thank Mr. G. MacAloney for his assistance and mechanical abilities. Others to whom I would like to extend my gratitude include, Mr. R. Slovik, Dr. M. Kamath., Miss J. MacAloney, Mrs. Y. Chen, and Mrs. C. Ford. Finally I would like to acknowledge the financial support provided by the National Science and Engineering Research Council.

TABLE OF CONTENTS

LIST OF FIGURES

LIST OF TABLES

LIST OF ACRONYMS

AR	Autoregressive
FIR	Finite Impulse Response
IIR	Infinite Impulse Response
LMS	Least Mean Square
RLS	Recursive Least Squares
STFT	Short Time Fourier Transform
PSD	Power Spectral Density
ECG	Electrocardiogram or Electrocardiograph
EGG	Electrogastrogram or Electrogastrograph
EMG	Electromyogram or Electromyograph
NANC	Non-Adrenergic Non-Cholinergic
VIP	Vasoactive Intestinal Peptide
Ach	Acetylcholine
GEA	Gastric Electrical Activity
NTS	Solitary Tract
DVC	Dorsal Vagal Complex
ATP	Adenosine Triphosphate

ADP	Adenosine Diphosphate
RMP	Resting Membrane Potential
ICC	Interstitial Cells of Cajal
TTX	Tetrodotoxin
NE	Norepinephrine
GRP	Gastrin Releasing Peptide
SP	Substance P

Chapter 1

Introduction

1.0 Problem Description

The study of stomach functionality and its relationship to electrical activity requires sensitive diagnostic and research tools. Currently much research in the area of gastric electrophysiology is being performed in-vitro, using well established, but limited, methods. The goal of this thesis was the development of a research tool which provides a means to record in-vivo electrical activity from the stomach. Processing methods were applied to extract useful information from the recorded signals. These tools and methods were extensively tested by several practical applications.

This research tool was designed to be as flexible as possible with the ability to be applied to the two main research topics in this area, clinical diagnostics and neurological control research. This system was able to record the electrical activity of the stomach from non - invasive skin mounted surface electrodes, as well as invasive serosal electrodes. Through experience with these recordings, investigations of their correlation with gastric function, and the development of more complex processing schemes, this tool may one day become a useful clinical diagnostic technique. As well, recordings from

the stomach wall will provide a representation of normal activity. By examining changes in this signal, in response to various stimuli, the neural control of gastric function may be examined. This may also have important significance, for example, in the development of a protocol for electrical pacing of the stomach. These important goals cannot be reached without properly developed tools and background work.

1.1 Overview

This thesis is focused towards providing a reference for future biomedical engineers, physicians, or electrophysiologists who may begin research in this area. A thorough summary of relevant background material is provided to ensure the proper framework and motivation for applied techniques and conclusions. Chapter 2 begins by giving a brief overview of the stomach and related aspects of electrophysiology. Chapter 3 introduces the recording system and discusses topics relating to signal recording. A detailed outline of the signal amplifier design is then provided in Appendix A. The applied signal processing techniques are summarized, with application examples, in Chapter 4. Chapter 5 provides several general comparisons between the electrical activity from different regions of the stomach and discusses the basis of these electrical characteristics. Finally, Chapter 6 applies the previously described background material, developed tools and signal processing techniques in a brief study of the nervous control of the stomach. The general flow of this thesis from background material to tools and

techniques and finally an applied research application, will hopefully provide readers with a thorough reference to aid in further research in this field.

Chapter 2

The Stomach

2.0 Introduction to The Stomach

2.0.0 Anatomy and General Function

The stomach is one of the main organs of the gastrointestinal tract, whose purpose is to store, process, and transport food. A bolus of masticated food, is emptied from the esophagus through the gastroesophageal sphincter into a part of the stomach known as the cardia. It is then ground and mixed with gastrointestinal secretions by the contractile force of the muscles of the stomach to form chyme. This is stored in the fundus, and emptied at a precisely controlled rate into the duodenum for digestion and absorption in the small intestine. Circular rings of muscle contraction, known as "constrictor rings", surround the stomach and move towards the pylorus every 15 to 20 seconds. These waves of contraction are responsible for gastric emptying.

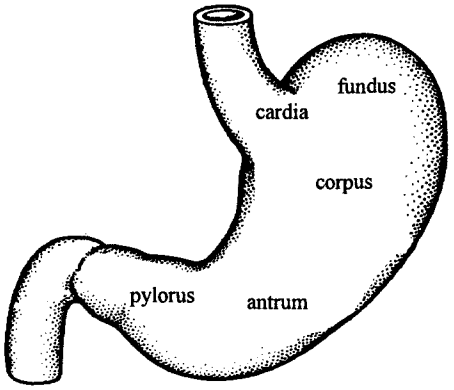

Figure 2.0: Regions of The Stomach

The stomach is divided into three main regions: the fundus, the corpus, and the antrum, as shown in Figure 2.0. Each region has distinct features and functions. The fundus, for example, has much thinner muscle layers and functions as a holding tank, relaxing to accommodate a larger volume when necessary. The corpus accepts newly swallowed food, and undergoes mixing actions. The frequency of the intrinsic pacemaker is highest in the orad corpus and thus is the site of origin of gastric electrical slow wave activity[4]. The antrum has an increasingly thick circular muscle layer and undergoes strong phasic contractions in peristaltic waves. This action moves chyme to the pylorus for both emptying, through the pyloric sphincter, and mixing, by retropulsion[2]. The pylorus has a very thick circular muscle layer and acts as a control valve, controlling the amount and rate of gastric emptying.

The stomach wall is made up of three distinct layers, the mucosal, the muscularis, and the serosal layers [1,2,4]. The mucosal layer is further divided into three sublayers: the mucosa, the muscularis mucosae, and the submucosal layer. The mucosa is an epithelial layer which lines the interior of the stomach, while the muscularis mucosae is a layer of low density smooth muscle cells, and the submucosal layer is layer of connective tissue interlaced with the enteric nervous system. The second layer, the muscularis, also consists of three sublayers: the longitudinal, the oblique, and the circular muscle layers. The longitudinal layer consists of two distinct sections, one section beginning in the esophagus and ending in the corpus, and the other beginning in the corpus and continuing into the duodenum [4]. The circular muscle layer is a continuation of the circular layer of

the esophagus and is present in all sections of the stomach with the exception of the fundus. The thickness of the circular layer increases distally, through the antrum, and ends, extremely thick, at the pylorus. It is this layer which is mainly responsible for the movement of the food and its emptying into the duodenum. The oblique layer is found in the fundus and near the lesser curvature of the stomach, but disappears distally. Finally, the serosa is the outermost layer of the stomach, a thin covering of areolar tissue covered by a single layer of squamous cells.

The stomach has several precise control mechanisms which maintain its important role in the digestive system. For example, the muscle in the fundus responds to stomach pressure by relaxing, allowing the storage of a greater volume of food. Also, the state of duodenal activity is mainly responsible for controlling the rate of emptying by sending signals through a feedback pathway to the pyloric sphincter. By controlling the contractile tone of the pyloric sphincter, chyme is emptied into the duodenum at a rate suitable for digestion and absorption. These examples illustrate how the stomach is controlled by both internal and external factors, allowing it to function as an integral art of the gastrointestinal tract. This control takes the form of complex mechanisms involving nerves of the enteric and autonomic nervous systems, electrical properties of gastric smooth muscle, pacemaker cells, rhythmic electrical activity and many other factors at several different levels.

2.0.1 Gastric Innervation

Innervation of the gastrointestinal tract is generally divided into intrinsic and extrinsic nerves. The intrinsic nerves are the nerves of the enteric nervous system, located throughout the layers of the stomach, while extrinsic nerves are the nerves of the autonomic system, both sympathetic and parasympathetic.

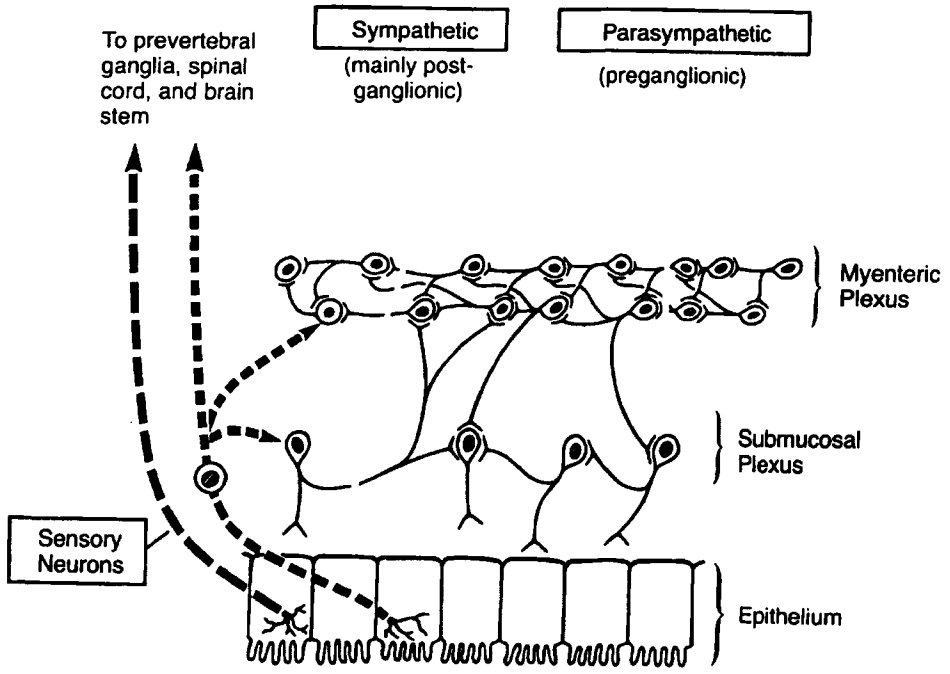

Figure 2.1: Basic Innervation of The Stomach [2]

2.0.1.0 The Enteric Nervous System

The gastrointestinal tract has such complex control mechanisms that it has its own nervous system, the enteric nervous system, illustrated in Figure 2.1. This nervous system is embedded in the layers of the organs of the gastrointestinal tract and consists of

an estimated 10 to 100 million neurons, roughly equivalent to the number of neurons in the spinal cord. Innervation is concentrated in several nerve plexi in the layers of the gastrointestinal tract. The two main ganglionated plexi are the myenteric plexus, found between the longitudinal and circular muscle layers, and the submucosal plexus, found in the submucosal layer. The myenteric plexus mainly controls gastrointestinal movements while the submucosal plexus controls gastric secretion and local blood flow and is much more predominant in the small and large intestines than in the esophagus and stomach. These layers are connected by many nerve fibers running through the intermediate layers. As well, several nonganglionated plexi are present. These include the longitudinal muscle plexus, the circular muscle plexus, the plexus of the muscularis mucosae, the mucosal plexus and a perivascular plexus found around arteries in the gut wall [(1)]. The longitudinal muscle plexus consists of nerve fiber bundles found throughout the thickness of the longitudinal muscle, running parallel to the muscle. The circular muscle plexus also consists of parallel nerve fiber bundles throughout the muscle. However, in some regions of the gastrointestinal tract, notably the small intestine, this plexus is separated into a thin inner layer and a dense outer layer. This outer layer is referred to as the deep muscular plexus [(1)]. This organization can vary considerably between different species.

The enteric nervous system is a complex structure consisting of several distinct neuron types, several distinct functional groups, and involves the influence of several major neurotransmitters. Although many distinct neuron types have been identified by physiologists, the two most notable classifications are the uniaxonal or AH type and the

multiaxonal Dogiel type II or S type neurons [1]. One notable difference is the effect of tetrodotoxin, a sodium channel blocker. The uniaxonal neurons are completely blocked by TTX while the Dogiel type II neuronal are not fully blocked. Established neurotransmitters used by these neurons include acetylcholine (Ach), norepinephrine (NE), gastrin releasing peptide (GRP), substance P (SP), and vasoactive intestinal peptide (VIP). Others of less understood but demonstrated presence exist and are listed in (1).

The neurons may also be classified by function into the following classes; excitatory muscle motor neurons, inhibitory muscle motor neurons, secretomotor

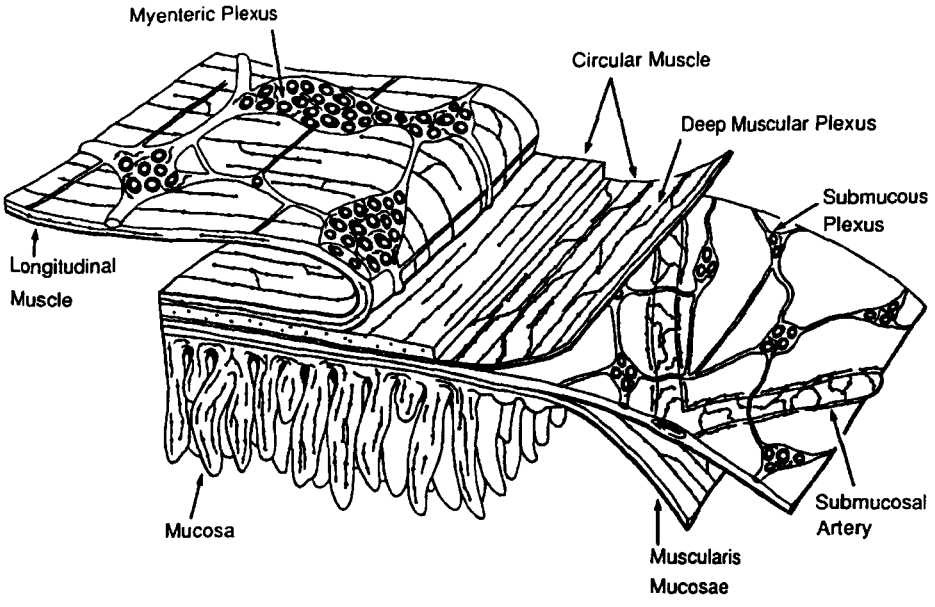

Figure 2.2: Innervation of Stomach Layers [1]

neurons, enteric vasodilator neurons, motor neurons to endocrine cells, enteric

interneurons, and intrinsic enteric sensory neurons [1]. Excitatory muscle motor neurons innervate the musculature of the stomach with acetylcholine acting on the muscle via muscarinic cholinergic receptors. Although acetylcholine is the principal neurotransmitter here, the tachykinins, substance P, and neurokinin A also contribute to excitation of the muscle. Inhibitory muscle motor neurons use vasoactive intestinal peptide (VIP) and possibly adenosine triphosphate (ATP) as transmitters. Secretomotor neurons controlling gastric acid secretion in the stomach and water and electrolyte secretion in the intestines, are cholinergic, acting on cells via muscarinic receptors. Enteric vasodilator neurons found in the intestines and possibly the stomach use an unknown neurotransmitter. Motor neurons to enteric endocrine cells are neurons located in the stomach wall which control the release of gastrin from gastrin cells by transmission mediated by gastrin releasing peptide. Enteric interneurons exist in the plexi of the enteric system and are probably cholinergic although evidence exists that (5-HT) 5-hydroxytryptamine also acts as a transmitter in the interneurons of the descending pathways of the small intestine. Finally there are intrinsic enteric sensory neurons which are sensitive to stimuli such as distention, luminal chemistry, and mechanical stimulation of the mucosa. These functional types of neurons are interconnected to form the complex structure of the enteric nervous system. As well, the enteric nervous system is interconnected with nerves of the autonomic nervous system, both sympathetic and parasympathetic.

2.0.1.1 Autonomic Nervous System

The autonomic nervous system exercises control over gastrointestinal function through both sympathetic and parasympathetic innervation. Autonomic nerves contain both afferent and efferent pathways. Afferent pathways transmit information from receptors in the effector cells to the brainstem, spinal cord, and prevertebral ganglia. Efferent pathways, on the other hand, are pathways from these centers to the stomach. Afferent pathways include the vagus (Xth cranial nerve) from the brainstem and sympathetic nerves, originating in T1 to L2 segments of the spinal cord. It is known that there is a direct sensory link from the muscle cells of the gut to the solitary tract (NTS) of the brain stem through (preganglionic) afferent vagal nerves which comprise the majority of the afferent innervation of the stomach. As previously mentioned, it is also known that there are intrinsic enteric sensory neurons which directly link the effector cells with the enteric system. However, it is uncertain if there is an afferent pathway between the enteric nervous system and the brain stem.

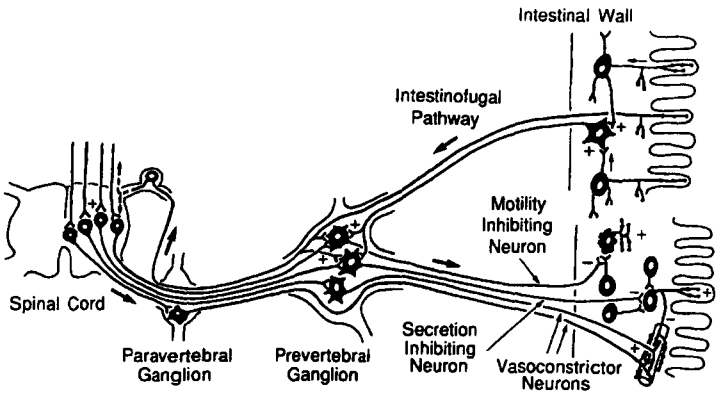

Figure 2.3: Sympathetic Pathways to the Stomach [1]

Efferent innervation is also by way of vagal and sympathetic nerves. In the dorsal vagal complex (DVC) of the brainstem, prevagal neurons from higher brain centers

synapse with interneurons from the afferent vagus in the NTS then forming an efferent vagal pathway to the enteric nervous system. These vagal neurons are preganglionic neurons located in the brainstem with axons traveling directly to the enteric system. Conversely, sympathetic innervation is a polysynaptic nervous pathway. Preganglionic neurons in the spinal cord travel either to prevertebral ganglia, the celiac ganglion for the stomach, or synapse with neurons in the paravertebral chain. From one of these sources, postganglionic neurons then pass to the enteric nervous system.

Preganglionic neurons including the vagal nerves and preganglionic sympathetic nerves are cholinergic, acting on nicotinic cholinergic receptors with the neurotransmitter acetylcholine. Postganglionic vagal nerves, the nerves of the enteric system, are also cholinergic, acting on the muscurinic cholinergic receptors of the effector cells and other enteric neurons. The effect of these neurons on the stomach is generally excitatory, increasing gastric motility and secretion. Postganglionic sympathetic neurons, on the other hand, are mostly adrenergic neurons, releasing norepinephrine as a neurotransmitter, while a small minority are cholinergic. Conversely to vagal innervation, sympathetic innervation is generally inhibitory, decreasing motility and secretion. Using these mechanisms, the autonomic nervous system exerts control over gastric function indirectly by its modulation of the enteric nervous system. Thus, alterations in gastric function, initiated by the autonomic nervous system, function by invoking changes in the enteric nervous system.

2.1 Physiology of Gastric Visceral Smooth Muscle

2.1.0 Anatomy of Smooth Muscle

The smooth muscle of the gut, unitary or visceral smooth muscle, consists of a syncytium of muscle fibers. That is, the muscle fibers are interconnected into sheets or bundles, closely coupling mechanical and electrical activity through membrane attachments and gap junctions so that the many muscle cells act together. The plasma membranes of the muscle cells have areas where dense bands in adjacent cells are in close proximity, called intermediate junctions, which couple the contractile mechanisms between cells. Gap junctions between cells allow the flow of ions [1,2]. The contractile mechanism in this type of smooth muscle is similar to that in skeletal muscle. Calcium ions cause the interaction of actin and myosin filaments, large polymerized protein molecules responsible for contraction, using energy derived from the conversion of ATP to ADP. The force of contraction is passed from dense bodies within the cytoplasm to dense bodies on the plasma membrane, via intermediate filaments. Although it is the

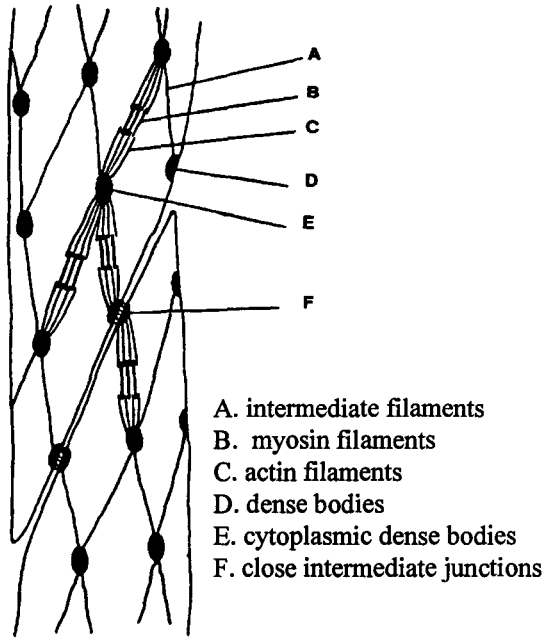

Figure 2.4: Gastric Smooth Muscle [1]

increase in intracellular calcium ions which causes contraction, the actual contractile mechanism is different than in skeletal muscle but shall not be discussed here [1,2]. The necessary change in intracellular calcium ions responsible for contraction is controlled by many mechanisms including neural stimulation, hormonal stimulation, stretch, and other factors. Smooth muscle cells have many different types of receptor proteins and even have inhibitory receptors, all which have a part in the control of calcium ion release and hence contraction.

These neuromuscular junctions are very different than those in skeletal muscle. Nerve axons have less branches and do not touch the muscle syncytium, but rather have multiple interruptions in the Schwann cells, varicosities, which allow the release of transmitter substances to travel to the receptors in the muscle cells which are in nanometer to micrometer proximity [1,2]. The transmitter substance diffuses to the muscle cells, often only to the outer layer. Muscle excitation can then be transmitted to inner layers by muscle action potentials. As mentioned, these junctions are both excitatory and inhibitory depending on the transmitter substance released from the axon.

2.1.1 Electrical Properties of Gastric Smooth Muscle Cells

Important to this thesis are the mechanisms controlling the contraction of this muscle directly as in neural stimulation, or indirectly by the alteration of membrane potentials, as well as, the electrical properties of the visceral smooth muscle cells and surrounding tissues of the stomach.

The resting membrane potential, RMP, of muscle cells is a point at which zero net ionic current crosses the membrane. This potential level is determined by the equilibrium of ionic concentration gradients and electrical charge gradients and is different for different regions and depths of the muscle layers of the stomach. The plasma membrane potential is regulated by many ion channels, the main ones being, voltage - gated Ca^{2+} channels, Ca^{2+} activated voltage - sensitive K^+ channels, non - selective voltage - gated cationic channels and ligand - gated channels. These channels represent different mechanisms for changing the membrane potential and are responsible for the electrical properties of the smooth muscle.

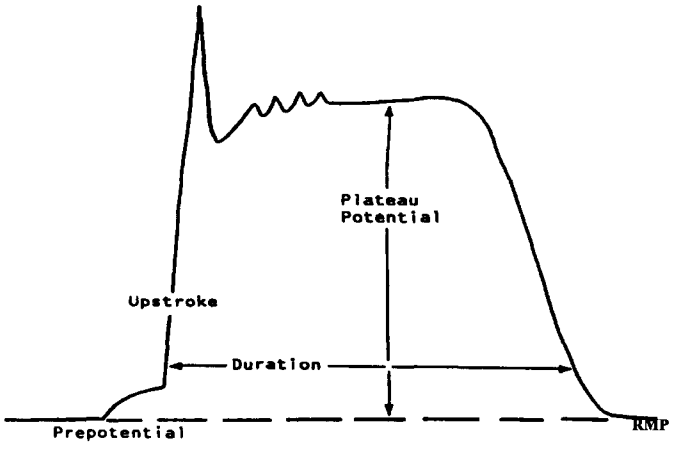

Figure 2.5: Ionic Slow Wave[1]

* scales indicative of different smooth muscle cells are shown in Figure 5.3

For reasons discussed below, visceral muscle cells of the gut undergo rhythmic electrical activity. This activity takes the general shape of Figure 2.5, the depolarization-repolarization wave, also known as a plateau potential, with variation in wave features depending on location and specifics of the particular muscle cell. In general, the wave begins with a prepotential, believed to be due to the non - selective voltage - gated cationic channels activating when stimuli raise the RMP above approximately -70 mV.

This is followed by a rapid upstroke depolarization, from an inward flow of Ca^{2+} through activated voltage - gated Ca^{2+} channels. These channels have a threshold of activation of -40 mV to +10 mV. These activated Ca^{2+} channels combined with the reverse effect of voltage - gated K^+ channels are responsible for the plateau region of the wave. As well as depolarizing the membrane, this inflow of Ca^{2+} ions also increases cytosolic Ca^{2+}. This increase eventually inactivates the Ca^{2+} channels and activates Ca^{2+} activated K^+ channels which induces an outflow of K^+ ions and suppression of inflow of Ca^{2+} ions. This action is responsible for the relatively rapid repolarization back to RMP. These mechanisms are not very well understood and may differ from region to region [1].

This depolarization - repolarization wave occurs rhythmically in the muscle layers of the stomach. This rhythmic activity has been termed the slow wave potential and has been studied quite extensively in humans. It has been observed that the intrinsic frequency of the muscle cell depolarization-repolarization wave decreases aborally, 3 to 5 cpm in the corpus while only 1.5 cpm in the antrum. RMP was also found to vary with location, -51 mV in the corpus and -71 mV in the antrum. Finally, the duration of the depolarization-repolarizaton wave has been observed as 5 seconds in the corpus while 20 seconds in the antrum. These differences are believed to be due to slight differences in muscle cell characteristics.

The site of origin of this rhythmic activity is also not well understood and some controversy exists. Interstitial cells of Cajal (ICC), also known as pacemaker cells, are known to be spontaneously active and are believed to be involved in the generation of the

rhythmic activity [3]. These cells have been found at the myenteric and submucosal borders of the circular muscle layer in the stomach and appear to make contact with muscle cells and are highly innervated. Is the rhythmic electrical activity an intrinsic property of gastric smooth muscle cells, or does the rhythmic activity come from interstitial cells of Cajal? There remains much uncertainty about the exact role of the interstitial cells.

The slow wave seems to originate in the myenteric and submucosal pacemaker regions. The slow waves propagate rapidly around the circular muscle due to an abundance of gap junctions in the circular muscle syncytium. Propagation also occurs in the longitudinal muscle layer, although slower due to less gap junctions. In this way, the slow waves propagate as discrete rings of excitation along the length of the gut in both oral and aboral directions. Propagation may occur in only one direction under two mechanisms. First, a higher intrinsic frequency and fast conduction velocity allows proximal sections to set the pace of more distal segments. Second, inhibitory neural input may limit propagation in a segment, preventing propagation in that direction.

Accompanying slow waves are much more rapid depolarization - repolarization waves known as spike potentials. These potentials have a period of 0.1 to 0.2 seconds and occur superimposed on slow wave potentials. Spike potentials are accompanied by muscle contraction although they are not essential for contraction.

It has been observed in the stomach that electrical activity in different regions occur for specific purposes. There is a proximal to distal gradient in RMP and as such the

RMP in the muscle cells of the fundus region is approximately -50 mV, which is near or above the threshold. For this reason, the fundus undergoes tonic contraction and is almost devoid of rhythmic activity. This tonic contraction, regulated by neural control allows the fundus to function as a "holding tank", contracting or relaxing to satisfy the needs of the stomach content. The corpus seems to have both tonic and phasic contractions, probably acting as an interface between the holding tank and the processor. The antrum, on the other hand, has very little tone and with the lowest RMP, is best suited for slow wave propagation. As well as propagating in the longitudinal direction slow waves also propagate transversely. In the pylorus, which has the thickest circular layer, the slow waves may even decay before they reach the innermost circular layer. This is believed to be responsible for the intrinsic tone of the pyloric sphincter [1].

This summary briefly describes how the characteristics of specific muscle cells generate the electrical activity responsible for some of the functionality of the stomach. By regulating these mechanisms both directly and indirectly with neural input, the functions of the stomach can be controlled. This control occurs at several levels, from very local reflexes involving only enteric neurons to high level neural pathways, involving enteric neurons, autonomic neurons, and neurons of the brain stem

2.2 Introduction to Electrogastrography

Electrogastrography is the study of the electrical activity of the stomach. Many researchers [2,4,6], have classified the gastric electrical activity into three components; electrical control activity (slow waves), electrical response activity (spike potentials), and resting potential shifts. The slow waves exist at an average frequency of approximately 3 cycles per minute in humans, slower in smaller animals. The frequency of these slow waves varies between subjects and under different conditions including abnormal gastric activity. The frequency range of this can be higher, 3.6 to 9.9 cpm in tachygastria or lower, 0 to 2.4 in bradygastria. Spike potentials are of much smaller amplitude and exist only on the crests of the slow waves. It has been determined that the occurrence of these spikes is directly related to contractile activity while the slow wave activity is related only indirectly by its control on the spike activity[2,7]. The relationship between these electrogastric signals, acquired from macroelectrodes, and the depolarization - repolarization waves of muscle cells, Figure 2.5, will be discussed in detail later. Samples of recorded electrogastric activity, under different recording conditions are shown in Figure 2.6. The electrogastric signal can vary greatly depending on a number of factors. The electrodes used to record the electrical activity and the recording location are the most important factors in determining signal quality. The two main, and very different, recording locations are on the serosa or stomach covering, and on the surface of the skin. Serosal recordings are the "gold standard", with signal levels ranging from 0.5 mV to 10 mV. These recordings allow for a much more detailed

representation of gastric electrical activity, with a higher signal-to-noise ratio. However, serosal implanted electrodes are invasive, requiring surgery, and therefore are not a viable clinical tool. Surface electrodes, on the other hand, are easily applied and truly non-invasive. However, the signal acquired from the surface, is a very different signal, consisting of electrical activity in the range of 10 to 500 μV. Volume conduction of the gastric electrical activity, from the stomach wall to the skin, as well as, the averaging effect of the relatively large silver-silver chloride electrodes, account for this difference.

There are several goals in the area of electrogastrography. First, researchers hope to develop a more complete understanding of the neural control of the stomach through the analysis of its electrical activity and changes that take place. A complete, detailed model of normal electrical activity and its relation to the functionality of the stomach, aids in this research. Unfortunately, the electrical activity of the stomach is not ideal for recording. The signal level is very low and there are many possible noise and artifact sources which lower the signal-to-noise ratio significantly. There are many sources of noise which contribute to these recordings. First, electrocardiographic activity is a dominant interference source. This well known quasi-deterministic, periodic signal represents the electrical activity of the heart and is present by the volume conduction of the body tissues. Motion artifacts and respiratory artifacts are also significant in some recordings. Slight disturbances to the electrode / skin interface, cause changes in the measured skin potential and thus shifts are superimposed on the recordings[5]. Other sources of noise include, small and large bowel activity, 60 Hz noise, and

electromyographic interference from abdominal muscles. For these reasons, there is a significant effort to develop better recording methods, signal processing techniques, and insights, in order that electrogastrography may one day be a powerful clinical tool in examining the functionality of the stomach. The specific areas of development include; the use of serosal recordings on animal models to develop a model for gastric electrical activity, and relating surface recordings, often referred to as EGG, to true electrical activity in order to develop techniques which utilize this information in a useful way.

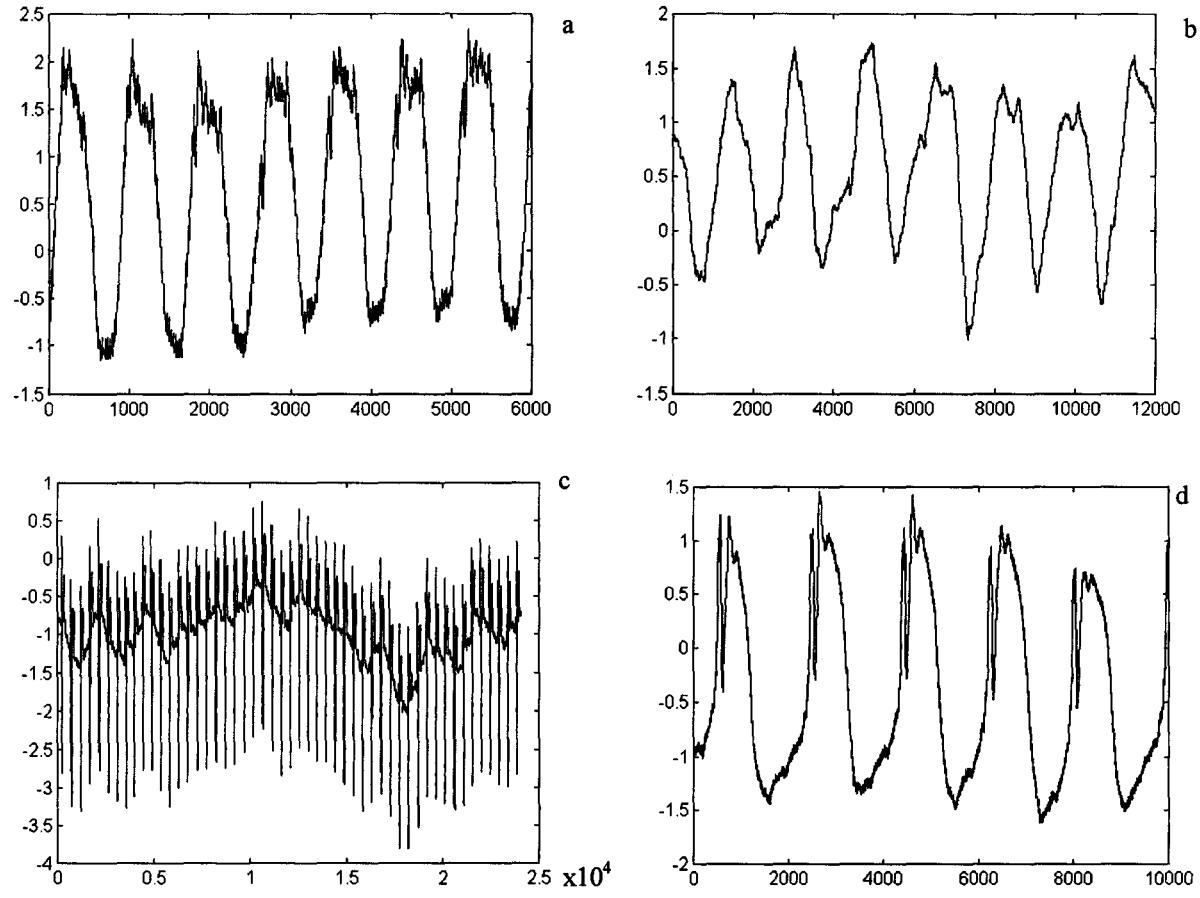

Figure 2.6: Examples of Recorded Electrogastric Activity a) recorded from serosa of human stomach with temporary myocardial electrodes, b) recorded from serosa of rat stomach using fine stainless steel wire, c) recorded from skin of human abdomen using Ag-AgCl electrodes, d) recorded from serosa of dog stomach with temporary myocardial electrodes.

* time axes are given in sample number while the vertical scale is in nominal recording units

CHAPTER 3

Data Acquisition System

3.0 System Overview

The system used for data acquisition is a simple biopotential recording system consisting of basic system building blocks. Figure 3.0, illustrates the overall signal pathway. Various electrodes are used to measure the electrical activity. These electrodes can be arranged in different configurations to record from different areas of the stomach. The electrical activity measured, as a time varying potential difference, is amplified by a signal amplifier with a differential front end. This amplifier features a variable gain, to account for the range of signal strengths, between serosal signals and surface EGG signals. Also, the amplifier incorporates a DC offset stage to compensate for internal offsets, as well as, possible polarization of the electrodes. To reduce noise and baseline drift while still including the best range of frequencies for gastric electrical activity, the amplifier is bandlimited from 0.01 Hz to 20 Hz. Details on the amplifier design are given in Appendix A. Next, the signal amplified to an appropriate level, determined visually, is connected to a codas data acquisition interface [26]. The signal is then stored in a codas data file, which can later be imported into analysis software.

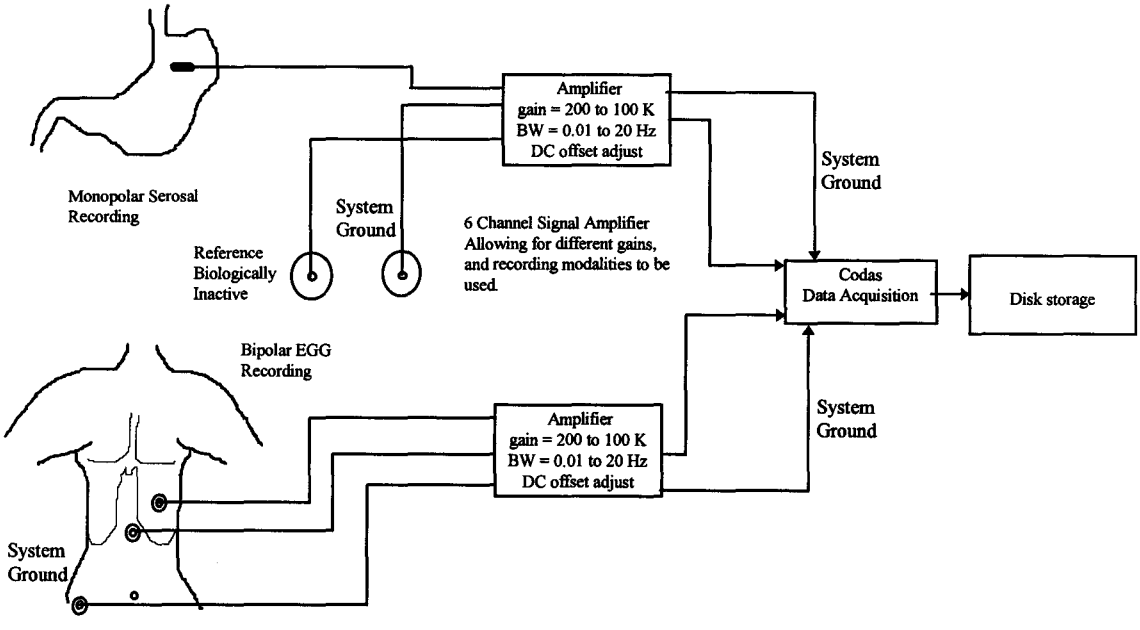

Figure 3.0: Data Acquisition System Overview

3.1 Sensing Electrodes

In the acquisition of electrogastric signals a number of different electrodes are appropriate in different recording paradigms. Cardiac Ag-AgCl electrodes, approximately 4 cm in diameter, were used for surface recordings where there is less size limitation but a higher importance on interface stability and impedence. Serosal recordings were done with teflon coated stainless steel wire of 127μm diameter and a bared length of 8 to 12 mm inserted into the serosa.

3.2 Noise Minimization

Great care was taken to minimize additive noise in the electrogastric signals through electrode parameter selection and apparatus. For the serosal recordings, impedance is reduced by keeping wire length minimal, approximately 3cm ($R=\rho L/A$). However, due to size limitations, since the stomach of a rat is very small, the required localization necessitated a very fine electrode wire with small cross sectional area (A) and contact length (L). Differences in electrode material leads to different half-cell potentials and a potential difference appearing across an electrode pair. This could cause current to flow and hence cause another source of noise. To reduce this possible effect, electrodes of the same material were used. As well, to reduce the effect of motion and hence instability of the electrode / electrolyte interface, an electrode positioning and securing apparatus was built to hold the electrodes in position.

60 Hz electromagnetic interference was reduced by use of lowpass filters, fc = 20Hz, in the signal amplifier, and by use of a Faraday cage for recordings. The inherent sensitivity of electrodes to parasitic capacitance was reduced by shielding the lead wires. Finally, the stomach serosa was kept well irrigated with parafin, a non-conductive liquid. This helped to maintain a consistently stable electrode / electrolyte interface with reduced levels of artifact.

Surface electrogastric recordings, recordings on the skin using Ag-AgCl electrodes, were made much more stable by abrasion of skin. The largest cause of motion artifact is mechanical disturbances of the electrode wire together with a high electrode

and skin impedance. By lowering the skin impedance, artifact is reduced significantly. The main source of the skin impedance is the stratum corneum and removing most of it by abrasion significantly reduces the skin impedance and hence artifact.

3.3 Electrode Arrangement

For serosal recordings where signal level is significantly greater than surface recordings, simple monopolar recordings yield acceptable results. Although a monopolar electrode arrangement is inherently more sensitive to biological noise sources it does not have the directivity limitations of bipolar recordings. This is useful for examining differences in GEA at different regions of the stomach. Bipolar recordings are more appropriate when signal levels are extremely low and only a sample of the electrical activity is required for overall classification or diagnostic purposes.

In the monopolar recordings, the active recording electrode was placed over the required site just under the stomach serosa. The ground electrode and reference electrodes were placed in biologically inactive sites on the right and left hind legs respectively. In this way, static buildup and various external interferences such as 60 Hz fields can be eliminated at the source by common mode rejection. The recorded signal will be a representation of the electrical activity at the active site with any sources of potential common to inactive tissue removed.

Chapter 4

Digital Signal Conditioning and Processing Techniques

This chapter introduces several very well established signal processing techniques which are applied here to electrogastric signals. The intent is to give a brief introduction of background theory for each technique. The technique is then illustrated by application to various electrogastric data sets, outlining specific details and benefits of the processing. Various aspects of time - series analysis, filtering, and spectral estimation will be presented.

4.0 Time - Series

4.0.0 The AR Model

The autoregressive (AR) model is a commonly used parametric model used to classify random signals and represent their expected structure. The autoregressive model predicts the current value of a discrete time series, x(k), as a weighted sum of past values, $x_k = -\sum_{n=1}^{p} a_n x_{k-n}$, where p is the model order. These parameters, **a**, are the autoregressive

model parameters and have several useful applications. The estimation of these parameters for a given data set, **x**, can be performed by several well developed methods such as the autocorrelation method utilizing the Yule-Walker equations or the Levinson-Durbin Algorithm [9, 11]. The solution to the Yule-Walker equations,

$$\begin{bmatrix} \hat{a}_1 \\ \hat{a}_2 \\ \vdots \\ \hat{a}_p \end{bmatrix} = -\begin{bmatrix} \hat{r}_0 & \hat{r}_1 & \cdots & \hat{r}_{p-1} \\ \hat{r}_1 & \hat{r}_0 & \cdots & \hat{r}_{p-2} \\ \vdots & \vdots & \ddots & \vdots \\ \hat{r}_{p-1} & \hat{r}_{p-2} & \cdots & \hat{r}_0 \end{bmatrix}^{-1} \begin{bmatrix} \hat{r}_1 \\ \hat{r}_2 \\ \vdots \\ \hat{r}_p \end{bmatrix}$$, using the biased sample covariance,

$\hat{r}_k = \hat{r}_{-k} = \frac{1}{N}\sum_{t=0}^{N-k-1} x_t x_{t+k}$, guarantees the stability of the estimated AR coefficients [11]. The variable, k, represents the lag number. The Levinson - Durbin algorithm is an efficient recursive procedure useful when the model order is large.

Autoregressive models were used to aid in the detection of changes in electrogastric signal characteristics. Using the identification procedure outlined in (10), the electrogastric signal was determined to be best represented by a 2nd order autoregressive model. By then tracking changes in autoregressive model parameters, it is possible to detect subtle changes in the signal which would not necessarily be detectable by other means.

4.1 Filtering

4.1.0 Digital Filtering

Digital filtering is used to reject specified frequency components of a signal while leaving others unaltered. In this way, it is possible to increase the signal to noise ratio and often completely isolate a particular component of a signal. Digital filters translate a discrete input signal to a filtered discrete output signal by a predetermined transfer function, describing the relationship between input and output. In the z-domain, $H(z) = \frac{X(z)}{U(z)}$, where H(z) is the transfer function. There are two distinct types of digital filters, finite impulse response (FIR) filters and infinite impulse response (IIR) filters. A FIR filter has a transfer function, $H(z) = b_0 + b_1 z^{-1} + \cdots + b_m z^{-m}$ which is always stable while an IIR filter has a transfer function, $H(z) = \frac{b_0 + b_1 z^{-1} + \cdots + b_m z^{-m}}{1 + a_1 z^{-1} + \cdots + a_n z^{-n}}$, stable when its poles are located within the unit circle in the z-plane. There are several methods for designing a digital filter with a desired transfer characteristic. These include the impulse invariant method, frequency sampling method and bilinear transformation [9]. Once the desired digital filter is designed, its transfer function is expressed in the previous form, filtering is simply the multiplication of the signal with the transfer function in the z-domain, $Y(z) = X(z)H(z)$. This function is equivalent to convolution in the time domain,

$$y(k) = (h * x)(k) = \sum_{m=-\infty}^{\infty} h(k-m)x(m).$$

In the time domain, the current output is expressed in terms of current and past inputs and past outputs:

$$y(k) = b_0x(k) + b_1x(k-1) + \cdots + b_mx(k-m) - a_1y(k-1) - a_2y(k-2) - \cdots - a_ny(k-n)$$

There are many characteristic transfer functions with different features, one of which is the butterworth response filter, with a maximally flat magnitude response in the passband. This ensures that all frequencies in the desired range are scaled by the same factor, not distorting the signal proportions.

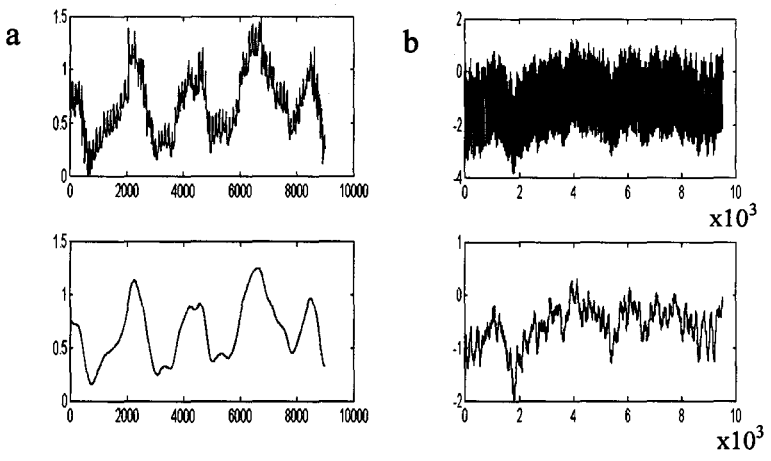

Figure 4.0: Application of Digital Filtering

a) filtering of respiratory artifact from rat GEA

b) filtering of ECG interference from surface EGG

* time axes are given in sample number while the vertical scale is in nominal recording units

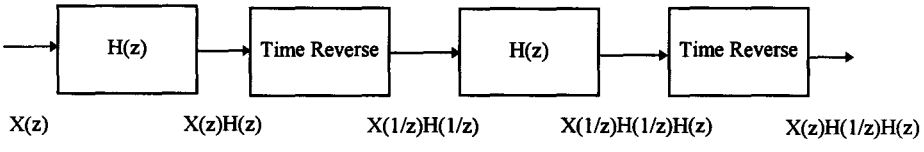

Figure 4.1: Scheme For Zero-Phase Filtering

In processing electrogastric signals, digital filtering was used to narrow the signal bandwidth when appropriate and remove several sources of artifact. The bandwidth of

the electrogastric signal amplifier, Appendix A, was designed to be 0.01 to 20 Hz, intentionally wider than commonly used electrogastric recording bandwidths, in order to include possible higher frequency control components and spike potentials. However, when examining effects on slow wave activity, it is beneficial to remove unnecessary frequency components. For this reason, examination of the rat slow wave signals, in chapters 5 and 6, included bandpass filtering of the signal to 0.02 to 0.2 Hz. As well, digital filtering was used in several instances to remove respiratory interference, cardiographic interference and motion artifact, examples illustrated in Figure 4.0. A 4^{th} order butterworth filter was designed as an IIR digital filter using Matlab's [25] "butter()" function. To ensure zero phase distortion, the "filtfilt()" Matlab function was used, which uses the algorithm outlined in Figure 4.1.

4.1.1 Adaptive filtering

Adaptive filtering, unlike ordinary digital filtering, is a type of time - varying filtering, in which the parameters of the filter change over time. In general, an adaptive filter applies some type of transformation to the input signal depending on the value of a set of parameters, which changes over time, based on some adaptation algorithm and signal statistics. A common filter structure is the transversal filter, illustrated in Figure 4.2. Common adaptation algorithms are the least mean square (LMS), recursive least square (RLS) and various fast least square algorithms. The simplest is the LMS which updates the tap weights according to, $\mathbf{w}_{j+1} = \mathbf{w}_j + 2\mu\varepsilon_j\mathbf{x}_j$. Where $\mathbf{w}$ is the weight vector,

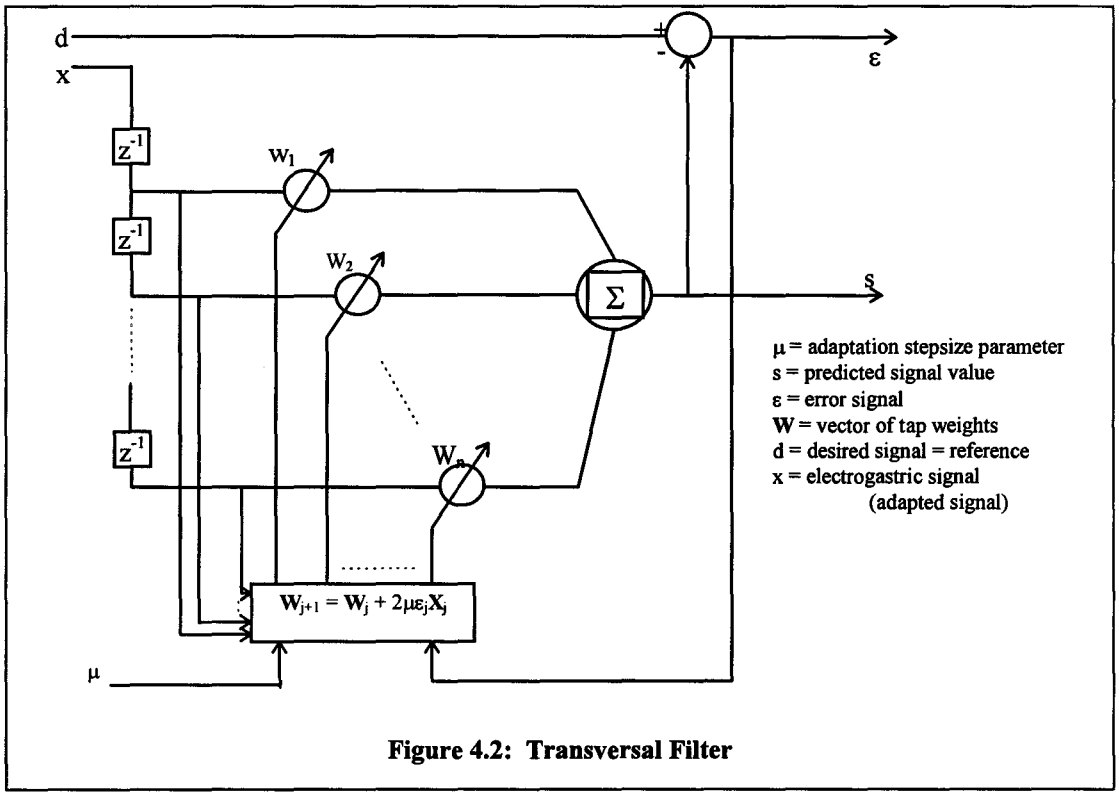

Figure 4.2: Transversal Filter

x_j is vector of past input values and ε_j is the error value, the desired value at iteration j minus the predicted value, $\varepsilon_j = d_j - \mathbf{w}_j^T \mathbf{x}_j$.

A common application is the removal of noise from a recorded signal. The reference signal is adapted by use of an adaptive

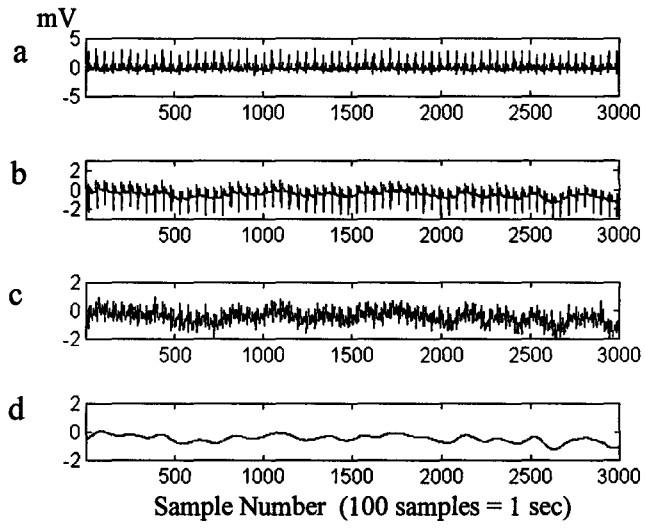

Figure 4.3: Adaptive ECG Interference Removal

a) ECG reference b) EGG signal c) LMS filtered EGG d) digital filtered comparison

filter to the correlated component in the recorded signal. Thus the error signal generated by this adaptation, the difference between the desired signal and the predicted noise component in the recorded signal, is the recorded signal with the noise removed. An obvious application of these adaptive filtering techniques to electrogastrography is the removal of ECG interference and respiratory artifact from EGG recordings for an increase in signal to noise ratio. This has the benefit of not removing other signal components which may be uncorrelated with the noise but still in the same bandwidth. This is often true of respiratory interference which is sometimes in the same bandwidth as slow wave activity under conditions of tachygastria. An example of this application is shown in Figure 4.3, which shows only a very marginal increase in signal to noise ratio. The signal to noise ratio is increased nevertheless, but due to practical difficulties in obtaining quality reference signals, the algorithm works less than ideally.

4.2 Spectral Analysis

4.2.0 Power Spectral Density

The power spectral density (PSD), defined by $S(\omega) = \sum_{k=-\infty}^{\infty} r_k e^{-j\omega k}$, represents the distribution of energy in the frequency domain. That is, the PSD is the Fourier transform of the covariance sequence of the signal. Practically, however, the PSD must be estimated due to the presence of only a finite set of data points. There are several

common approaches to the estimation of the PSD including the two discussed here, the periodogram method and the autoregressive spectrum.

4.2.0.0 Periodogram Method

The periodogram is an estimate of the true power spectrum obtained from a finite data set. The periodogram is defined by, $I(\omega) = \frac{1}{N}\left|\sum_{t=0}^{N-1} x_t e^{-j\omega t}\right|^2$,or alternatively,

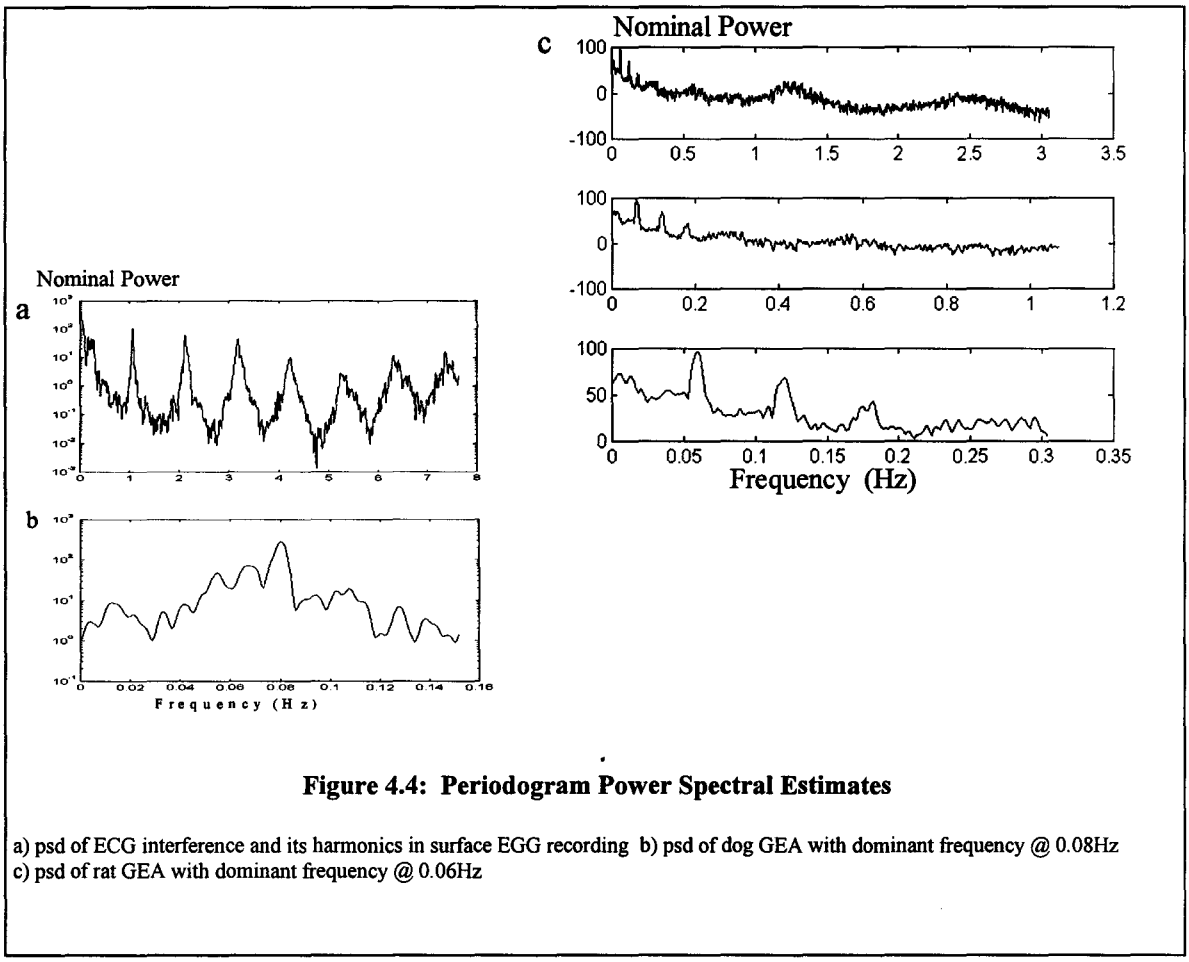

Figure 4.4: Periodogram Power Spectral Estimates

a) psd of ECG interference and its harmonics in surface EGG recording b) psd of dog GEA with dominant frequency @ 0.08Hz
c) psd of rat GEA with dominant frequency @ 0.06Hz

$I(\omega) = \sum_{n=-(N-1)}^{N-1} \hat{r}_n e^{-j\omega n}$, and is real and nonnegative, as is the true power spectrum [11]. The variables ω, and N represent angular frequency and number of samples respectively. The periodogram may be computed efficiently, using the Fast Fourier Transform, for frequencies , $\omega = 2\pi m / N$, $-N/2 + 1 \leq m \leq N/2$. The periodogram has been proven to be asymptotically unbiased, but is not a consistent estimate of the power spectrum, suffering from large variance. There are several methods of improving upon this periodogram to make it a useful estimate of the true power spectrum. These include averaging, smoothing, and windowing.

Averaging involves reducing the variance by segmenting the data set into equal sub-sets and calculating the periodogram as an average of the periodograms of the sub-sets. Given that the data set, N, is segmented into N_2 sub-sets of N_1 data points, the variance is reduced significantly. The reduction in variance is at the cost of reduced spectral resolution since there are now less points in each sub-set. It is also common to divide the data set into overlapped segments, allowing similar reduction in variance at less cost to resolution. Another way of achieving a similar effect is by periodogram smoothing. This involves the averaging of close data points of a single periodogram according to some set of weights. Windowing is another common enhancement technique. By using data windows more appropriate than a simple rectangular window, dispersion of power into sidelobes may be avoided and a closer estimate of the true power

spectrum obtained. Zero padding, interpolation in the frequency domain, may also be used to increase spectral resolution.

The periodogram method, implemented in Matlab [25] with the "psd" function was used to determine the frequency components of the recorded gastric electrical activity. Figure 4.4 shows several examples of estimated power spectrums.

4.2.0.1 Autoregressive Spectrum

This method estimates the power spectral density of a signal from the signal's autoregressive model parameters. First, the autoregressive model parameters are calculated by the methods described previously. The theoretical power spectral estimate of the autoregressive process is given by [14], $\hat{S}_{AR}(\omega) = \frac{\hat{\sigma}^2}{\left|1 + \sum_{k=1}^{p} \hat{a}_k e^{-j\omega k}\right|^2}$. This may be calculated efficiently using the FFT. A comparison between the electrogastric spectral estimates provided by the periodogram method and by the autoregressive method is illustrated in Figure 4.5. The periodogram spectrum was calculated in Matlab using, psd (rate114(1:120000), 2^16, 100, Hanning(2^15), 2^14). That is, a 50% zero - padded, Hanning windowed, 50%

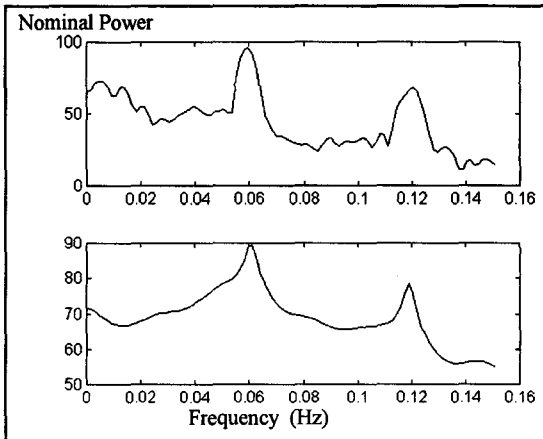

Figure 4.5: Comparison of Periodogram Method and AR Method

overlapped, average periodogram was calculated. The autoregressive spectrum was computed using freqz (1, lpc (10000, 5000), 2^15, 100). This first calculated the autoregressive parameters using the Levinson - Durbin algorithm, then calculated the theoretical spectrum with these parameters.

4.2.1 Time - Frequency Spectra

A common requirement is to examine how the frequency distribution of a signal changes over time to detect possible changes in the underlying physical process responsible for generation of the signal. Two common approaches are the Short - Time Fourier Transform and the adaptive autoregressive spectrum.

4.2.1.0 Short - Time Fourier Transform

The short - time Fourier transform (STFT) is an attempt at estimating the instantaneous frequency distribution of a signal using the Fourier transform and a subset of the signal to represent the signal at a particular moment of time. The signal is multiplied by a sliding window representing different moments in time, the product being Fourier transformed to give a representation of the power spectrum at that time. In this way, a time - frequency distribution estimate is calculated to represent the changing frequency characteristics over time. The STFT as a function of time and frequency is

represented by: $Y(t,f) = \int_{-\infty}^{\infty} y(s)\gamma(s-t)e^{-j2\pi fs}ds$. For a complete discussion of the STFT the reader is referred to (11).

The obvious trade - off is between spectral resolution and temporal resolution. Increasing the window length increases the spectral resolution but reduces the temporal resolution and has a time - frequency averaging effect, reducing the ability to detect fast frequency variations. A possible remedy is the use of zero padding, which increases spectral resolution by interpolation without the detrimental effects of an increased window size [13]. Too much zero padding, however, does not allow clear frequency peaks in the electrogastric signals to be recognized. Thus, the most appropriate choice depends on the particular characteristics of the signal being used. In particular, when applied to electrogastric signals, a window size of 4 minutes with zero padding of equal length was used to capture the important low frequency components of the signal and a time window shift of 1 minute was applied [12]. As with the periodogram, methods may be applied to reduce the variance of the STFT, however again at the cost of reduced spectral resolution. Examples of the time - frequency distributions of gastric electrical activity are illustrated in Figure 4.6, a 3D surface plot and Figure 4.7, a gray scale 2D plot.

4.2.1.1 Adaptive Autoregressive Spectrum

This method uses an autoregressive model, as described in section 4.1.0.1, to estimate the power spectrum of the signal. However, the model parameters are continuously adapted to the changing characteristic of the signal using an adaptive transversal filter, as in Figure 4.8. This allows the model to capture changes in the frequency distribution of the signal and gives a time - frequency distribution estimate for the signal. This method is better suited to track fast frequency variations than is the previous method [13]. The adaptive AR spectra for the signal of Figures 4.6 and 4.7 is shown in figures 4.9 and 4.10.

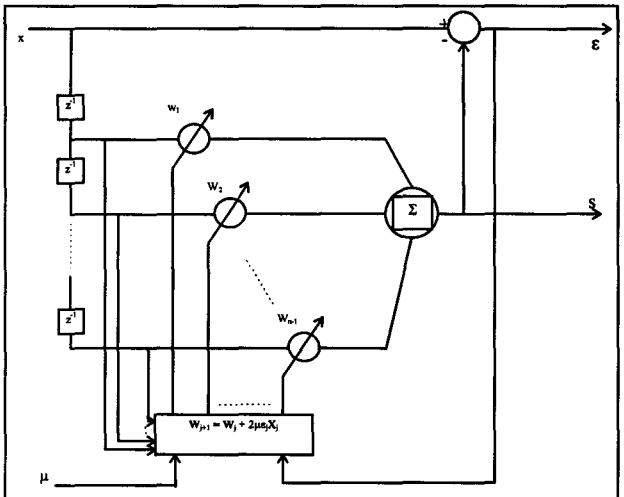

$$y_j = \sum_{k=1}^{p} a_{kj} x_{j-k} = \begin{bmatrix} a_1 & a_2 & \cdots & a_p \end{bmatrix} \begin{bmatrix} x_{j-1} \\ x_{j-2} \\ \vdots \\ x_{j-p} \end{bmatrix}$$

Where:

$$e_j = x_j - y_j$$

$$a_{k(j+1)} = a_{kj} + 2\mu e_j x_{j-k} \qquad k = 1,2,\ldots,p$$

Figure 4.8: Adaptive AR Coefficient Estimation

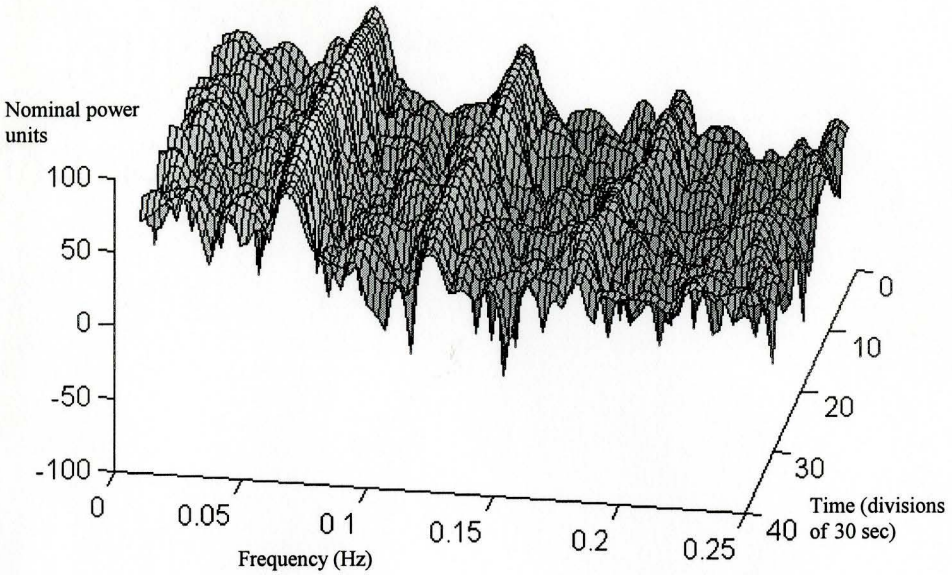

Figure 4.6: Sample STFT Spectrum 3D Plot

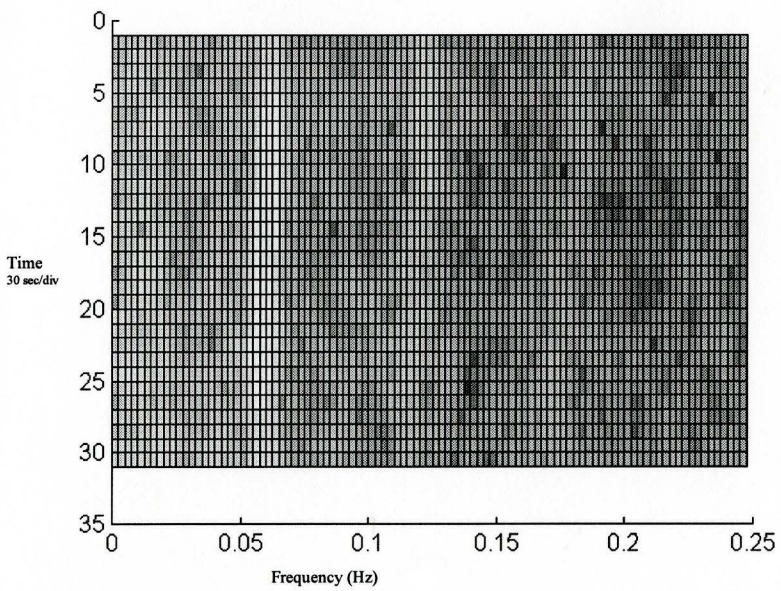

Figure 4.7: Sample STFT Spectrum Grayscale Plot

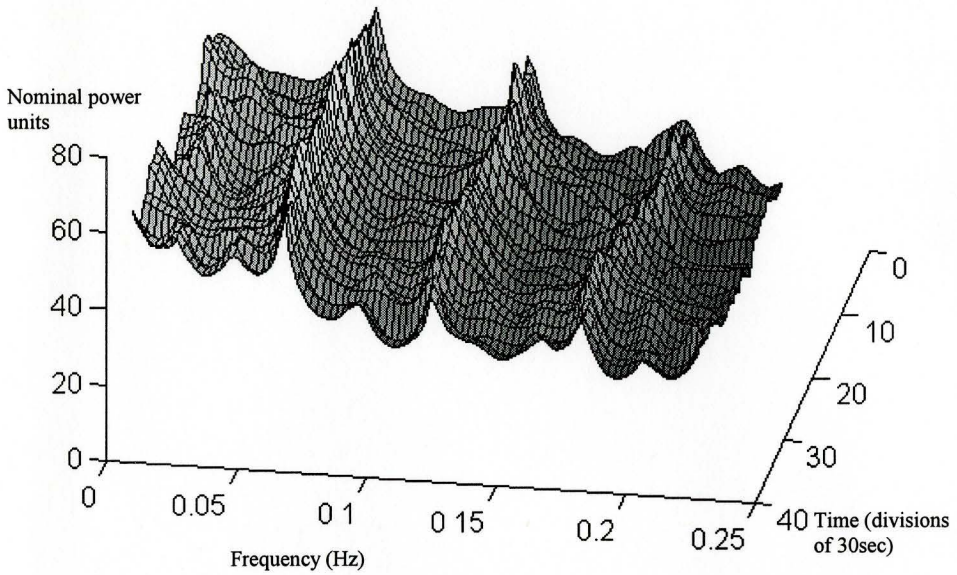

Figure 4.9: Sample Adaptive AR Spectrum 3D Plot

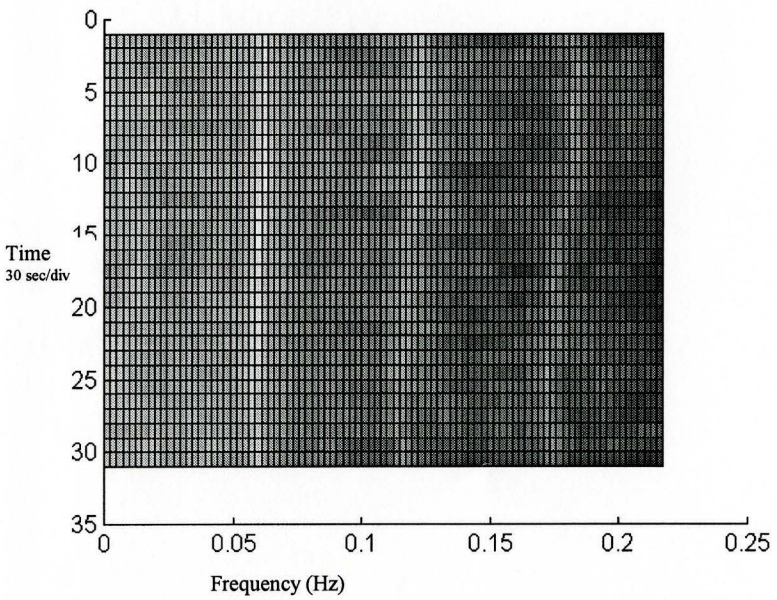

Figure 4.10: Sample Adaptive AR Spectrum Grayscale Plot

4.2.2 Cross Spectral Analysis

4.2.2.0 Cross Spectrum

The cross spectrum illustrates the frequency relationship between two signals. Defined as, $S_{xy}(\omega) = \sum_{m=-\infty}^{\infty} R_{xy}(m)e^{-j\omega m}$, where R_{xy} is the cross correlation for signals x and y, the cross spectrum may be estimated by application of the previous power spectral estimation methods. The cross correlation must be estimated from the sample correlation, $R_{x,y}(m) = \sum_{n=0}^{M-|m|-1} x(n)y^*(n-m)$.

The magnitude cross spectra of multichannel electrogastric recordings is useful for comparison of frequency components, as illustrated in Figure 4.11. As well, by examining the phase of the cross spectrum at the dominant electrogastric frequency, it is possible to determine an estimate of the time delay for the dominant frequency component between the two channels. This then provides an estimate of the slow wave propagation delay between the two electrode locations and consequently, the average propagation velocity.

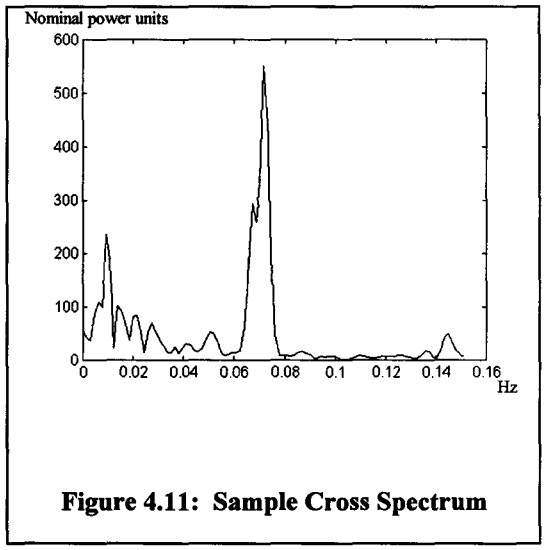

Figure 4.11: Sample Cross Spectrum

4.2.2.1 Coherence Spectrum

Another useful spectrum is the coherence spectrum, defined as,

$C_{xy}(\omega) = \frac{|P_{xy}(\omega)|^2}{P_{xx}(\omega)P_{yy}(\omega)}$. The coherence spectrum is real valued between 0 and 1, representing the correlation between the signals x(n) and y(n) at frequency ω. Figure 4.12 provides a sample coherence spectrum of a rat electrogastric signal.

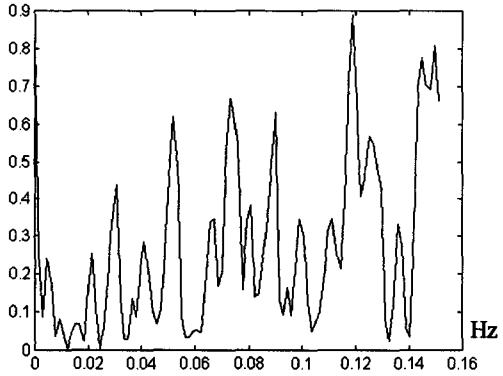

Figure 4.12: Sample Coherence Spectrum

Chapter 5

Gastric Electrical Activity

5.0 Relationship Between Cellular Depolarization-Repolarization Waves and Extracellular Recordings

5.0.0 Basis for Recorded Signals

The depolarization - repolarization wave which excitable gastric smooth muscle cells undergo when properly stimulated, is seen in Figure 2.5, and will be referred to as a plateau potential. This rhythmic change in membrane potential is distinct from the combination of electrical activity and fields which comprise in-vivo, extracellular recordings. For purposes here, the spatially integrated wave, comprised of a combination of plateau potentials, will be referred to as a slow wave and the combination of these slow waves and other recorded electrical phenomena will be referred to as gastric electrical activity (GEA). It is important to investigate the relationship between these cellular level transmembrane potentials and the in-vivo, extracellular, serosal recordings. Small variations in muscle cell electrical characteristics could lead to significantly different slow wave recordings, which allows us to study changes in gastrointestinal functional characteristics by examining gastric electrical activity.

Figure 5.0 schematically represents the smooth muscle syncytium by a number of rows of connected muscle cells (ovals). These cells are electrically coupled by several mechanisms including gap junctions. Slow wave propagation occurs by way of these electrical coupling mechanisms. A proximally located muscle cell is excited by some external stimulus to a point above its electrical threshold. The cell's membrane then undergoes the depolarization - repolarization cycle, plateau potential, described in section 2.1.1. As the cell undergoes this depolarization-repolarization of its membrane potential, it provides an external stimulus for neighboring cells, raising their membrane potentials by conduction through gap junctions. This eventually causes this more distal muscle cell to undergo depolarization-repolarization of its membrane, thus propagating the plateau potential.

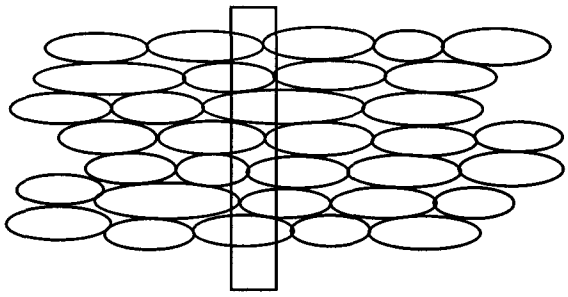

Figure 5.0: Recording from Muscle Cell Syncytium

It is quickly apparent that many factors determine this propagation of electrical activity and even more factors, involving the recording electrode configuration, determine the recorded signal characteristics. Factors which directly affect electrical activity include, muscle cell size, muscle cell proximity to each other, electrical coupling, electrical threshold, resting membrane potential, plateau potential duration, and other external stimuli. Other factors which indirectly affect the recorded signal by changing the

sensing characteristics of the electrode are electrode size (with respect to muscle cell size, resulting in spatial integration), electrode orientation (with respect to the muscle syncytium and wave propagation) and electrode filtering characteristics.

The size of the muscle cell with respect to the electrode size, determines the number of electrically active muscle cells which will be in close proximity to the electrode. The average muscle cell is about 400 μm long and 5 μm wide [1]. When this is compared to the serosal electrode size, about 5 mm in length and 127 μm in diameter, we see that many muscle cells contribute to the signal sensed by the electrode. Given these approximate dimensions, we know that if the electrode was positioned perpendicularly to the long axis of the muscle cell, it would cover approximately 1000 muscle cells along its length. This is illustrated, although compressed in number of cells, in Figure 5.0.

The muscle cells proximity to each other in the syncytium is another determining factor. Muscle cell size and shape vary slightly causing some randomness and irregularity in the structure of the muscle syncytium. This, in turn, causes some irregularity in the propagation of the plateau potential among the cells in the syncytium. Although the wave propagates in the same global direction, there are local variations and lack of completely synchronous propagation along the length of the muscle cells.

Electrical coupling between cells is also an essential determinant of electrical activity. In circular muscle the main coupling mechanism is through the abundant gap junctions, which allow quick exchange of ions between cells. This accounts for the relatively fast propagation in the circular muscle layer when compared to propagation in

the longitudinal muscle. The longitudinal muscle layer seems devoid of gap junctions [1] but still maintains coupling by other mechanisms. By examining Figure 5.0, it is clear that tighter coupling mechanisms which allow quicker excitation of neighboring cells, would alter propagation velocity and profoundly change recorded signal characteristics. As well, the electrical threshold and resting membrane potential of the muscle cells would also change propagation velocity and hence signal characteristics. A lower threshold or higher resting membrane potential would cause the cells to require less external stimulus to elicit a depolarization-repolarization cycle of the membrane potential.

The characteristics of the plateau potential also determine the recorded signal. As stated, the recorded signal is an integration of many muscle cell membrane potentials throughout a region near the electrode. Thus the electrical activity of each of these cells contributes to the overall recorded signal. The height of the peak of the plateau potential, the shape of the wave and the wave's duration, all effect the actual recorded signal. For example, if the plateau potential duration is increased, more cells will be excited in the proximity of the electrode at the same time and a larger slow wave signal will be recorded. However, the recorded slow wave will also be wider since it will take cells longer to repolarize back to their RMP.

Electrode characteristics are also an important signal determining factor. As stated previously, the electrode's size, with respect to the size of the muscle cells, determines the number of different cells' electrical activity which will be integrated into the recorded signal. Orientation of the electrode with respect to the propagation direction

of the slow wave is also crucial. Since the electrode passes over many muscle cells, all parts of the electrode may not measure propagated electrical activity at the same time. Other factors such as electrode filtering characteristics will also affect signal shape and amplitude. By knowing the relationship between cellular electrical activity and recorded signals, it is possible to explain physiologically, the changes in recorded gastric electrical activity.

5.0.1 Simulation of In-Vivo, Extracellular Recordings

A very crude simulation of the in-vivo extracellular recordings was performed to visualize the hypothetical relationship between the plateau potential of single cells and the actual recorded slow wave signals. A piecewise linear estimation of the plateau potential, Figure 5.1, was constructed and this electrical activity was simulated to propagate along a single chain of muscle cells assumed to have identical length. At each point in time the recorded signal was calculated as a weighted sum of influences from local muscle cells. Cells were weighted progressively smaller with increasing distance from the electrode, by some specified weighting function, Figure 5.2. In this way, a crude visualization is shown of the actual signal acquired from an electrode with electrical activity propagating down a chain of muscle cells, Figure 5.3 to Figure 5.6. To account for the many muscle cells found along the length of electrode, the final recorded signal is simulated as a sum of several of these chains of muscle cells; an example is illustrated in Figure 5.7. In this simulation, to account for slight offsets in longitudinal structure,

offsets in wave propagation were allowed for each chain. Electrode orientation is simulated by several chains of muscle cells with increasing offsets in waves since an electrode angled in the direction of propagation would receive the propagating wave at slightly different times along its length. Finally, degree of coupling is simulated by incorporating some source of randomness in the propagation of the plateau potential. This is shown, for example, in Figure 5.8, which is similar to actual recorded extracellular slow waves.

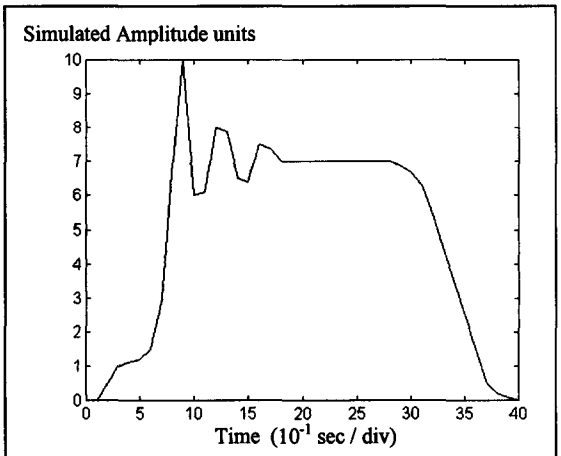

Figure 5.1: Simulated Depolarization-Repolarization Wave (Plateau Potential)

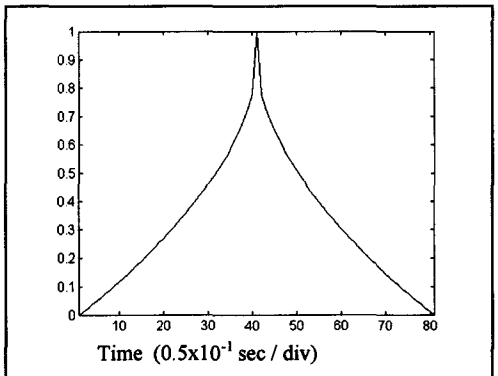

Figure 5.2: Sample Weighting Function

Several general changes in simulated signals were observed as a result of changes in one of the aforementioned factors. Most generally, it was observed that an increase in

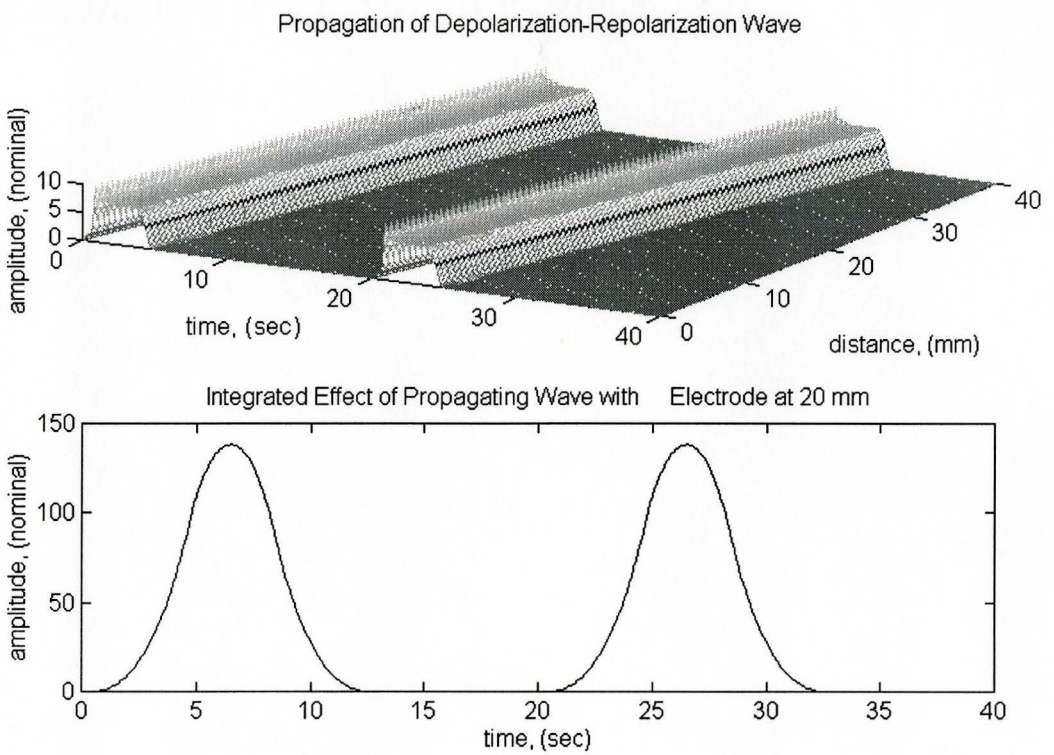

Figure 5.3: Simulation 1: (Normal)

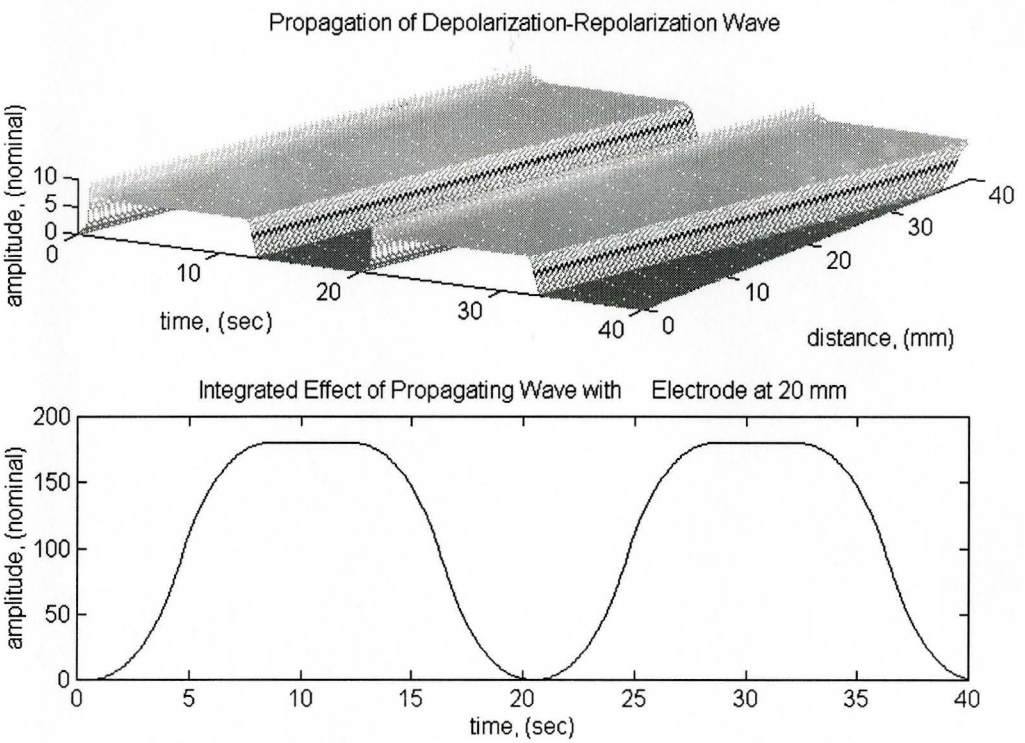

Figure 5.4: Simulation 2 (Long Plateau Duration)

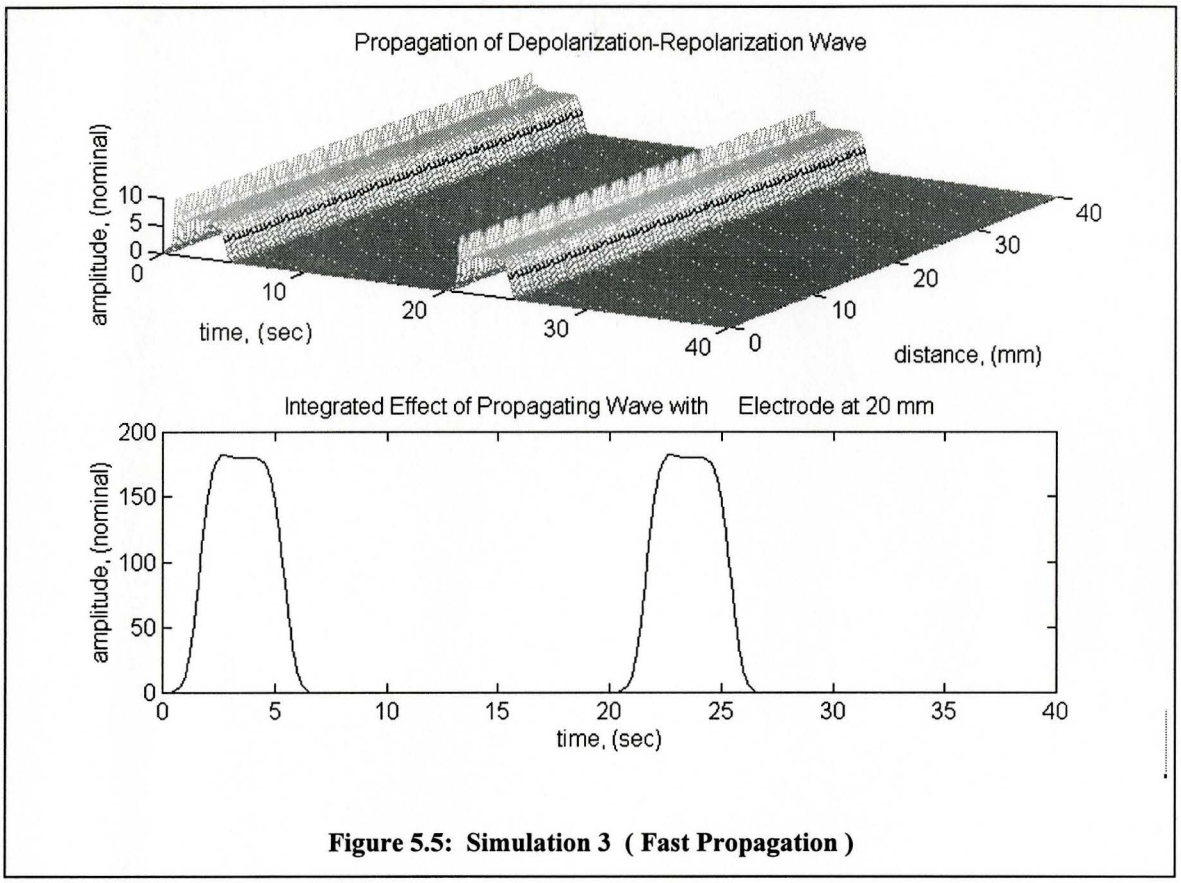

Figure 5.5: Simulation 3 (Fast Propagation)

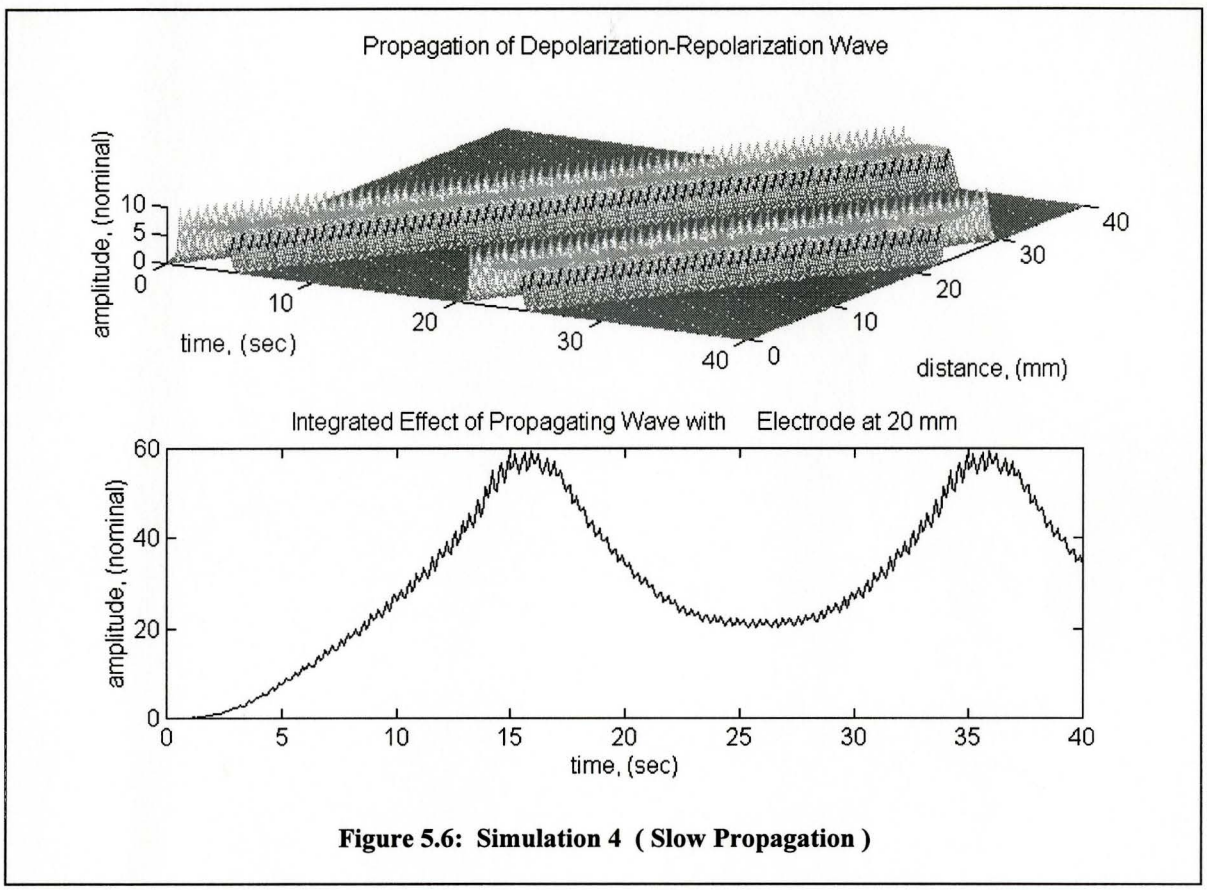

Figure 5.6: Simulation 4 (Slow Propagation)

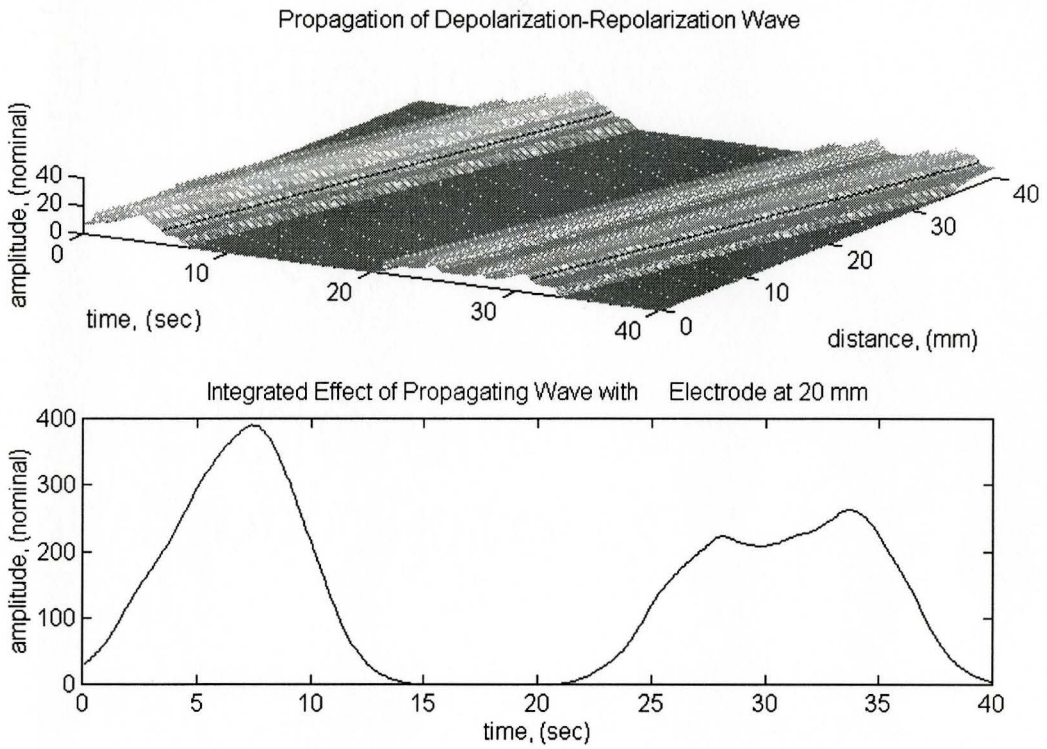

Figure 5.7: Simulation 5 (Offset Waves)

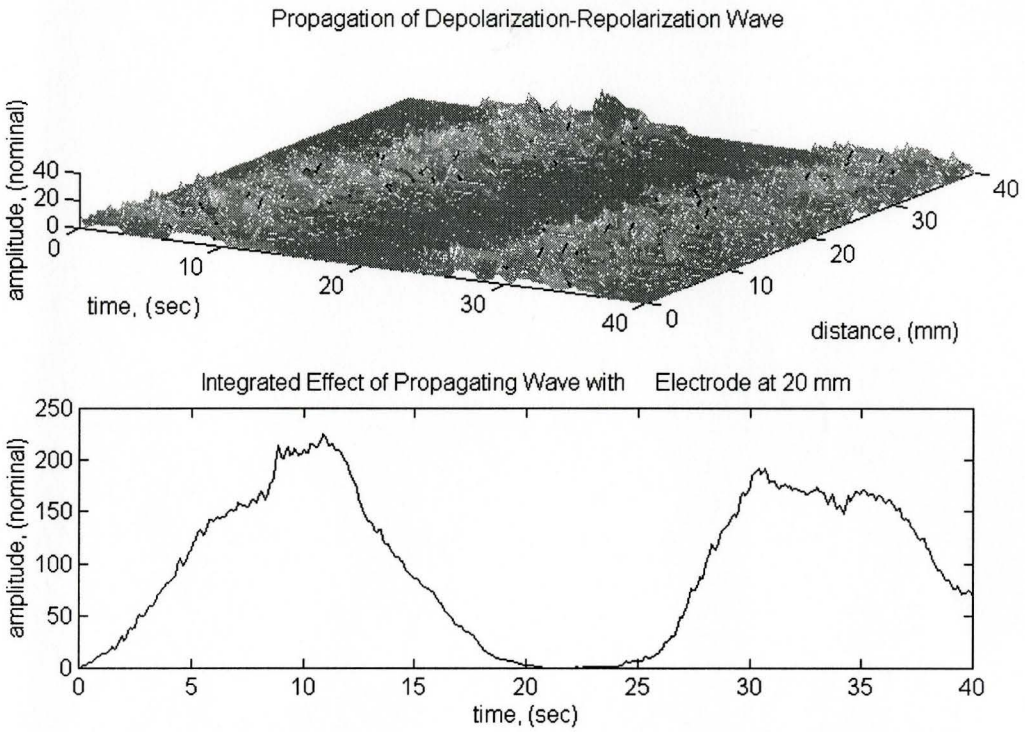

Figure 5.8: Simulation 6 (Loose Coupled Propagation)

plateau potential duration resulted in an increase in power of simulated slow wave signal, with both amplitude and width increased, as would be expected. However, it was also noticed that above a certain point this slow wave widened enough to "collide" with the next slow wave, resulting in a DC baseline . This actually reduced the slow wave variance because the signal is AC coupled. As well, a decrease in variance was also observed with a decrease in wave propagation velocity, Figure 5.5 versus Figure 5.6. A faster traveling wave causes the cells in the vicinity of the electrode to undergo depolarization-repolarization at nearly the same time, resulting in a slow wave which appears more like a plateau potential. A dramatic decrease in propagation velocity causes successive slow waves to collide, further decreasing variance. The orientation of the electrode with respect to the direction of propagation also affects the simulated signal. An electrode angled to the direction of propagation will have different portions of the wave front pass over it at different times, causing yet another form of spatial integration of the single plateau potentials. An example of how this might change the recording is shown in Figure 5.7 Finally, the degree of electrical coupling may also introduce some randomness into the signal, as in Figure 5.8.

Taking these factors into consideration, it is easy to visualize how serosal recorded GEA, with additive noise and motion artifact, may look very different than plateau potentials. However, knowing the relationship between the two may provide insight to changes taking place at the cellular level.

5.1 General Description of GEA Recorded From Rat Stomachs

Bioelectric signals, recorded from the stomachs of rats using teflon coated stainless steel electrodes have several distinct features. These signals are a summation of many signal components, biological, artifactual, and noise related. The strongest component of these signals is the gastric slow wave described extensively in the previous section. The dominant frequency of this component varies between subjects, usually in the range of 0.05 to 0.07 Hz (3 to 4.2 cpm), slightly faster than the human stomach, and may vary slightly over long periods. This component appears in most regions of the stomach to varying degrees.

Another predominant signal component is respiration artifact, occurring regularly in the frequency range of 0.8 to 1.6 Hz. This artifact is due to electrode and wire motion, impedance changes, and changes in the electrode - electrolyte interface. For this reason, the amount of respiration artifact is highly variable between electrodes. Depending on the state of the subject, the presence of larger, less frequent artifacts have been observed, and were determined to also be respiration artifact caused by periodic large gasps of air.

Other components of the recorded signal include electrocardial interference, other forms of motion artifact, and very low frequency variations in baseline level, the basis of which is unknown. These components may not be as striking as the previous, but are seen in some signals and must not be mistaken for GEA. It is also important to recognize the many areas of possible variation between recordings, which contribute to differences in recorded GEA signal. These include; physiological differences between rats,

anatomical differences between rats, level of anesthesia, amount of food present in stomach, anatomical placement of electrodes, orientation of electrodes, size and depth of electrodes, and other differences. Therefore, statistical inference methods are often necessary to prove significance of observed trends.

5.2 Regional Comparison of GEA

We know from previous research [1] that intrinsic electrical properties of smooth muscle cells differ between regions. Figure 5.9 shows samples of in-vitro transmembrane recordings of the plateau potential from different regions of the stomach. This suggests that in-vivo extracellular recordings of slow waves should also exhibit some differences between regions. However, this may not be a simple relationship since there are many more factors in-vivo, such as neural input, intact muscle syncytium, and propagation of pacesetting potential. For example, when the stomach is intact, the higher frequency of plateau potentials propagates along the syncytium, thus increasing the frequency in more distal regions from their intrinsic frequency.

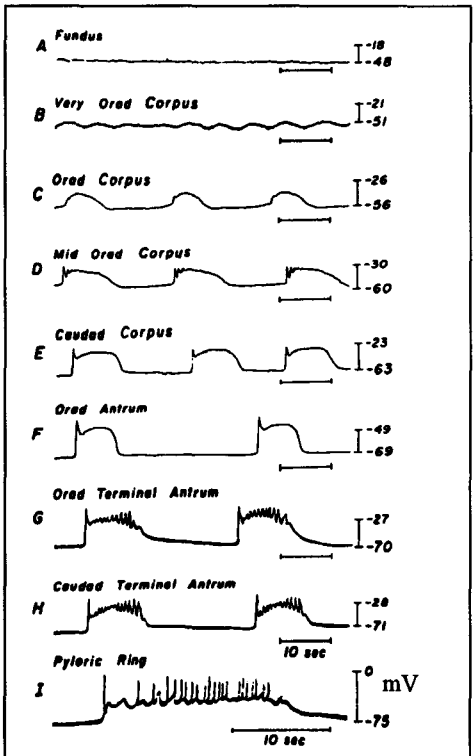

Figure 5.9: In-Vitro Plateau Potential Recordings [1]

5.2.0 General Comparison

Very generally, the fundus GEA was observed to be much less regular. The waveshape varies greatly, there is a much less predominant slow wave component and there seems to be much more inherent randomness in the signal. This irregularity decreases distally, the corpus recordings, in general, having a stronger slow wave component and less randomness. This trend continues into the proximal and distal

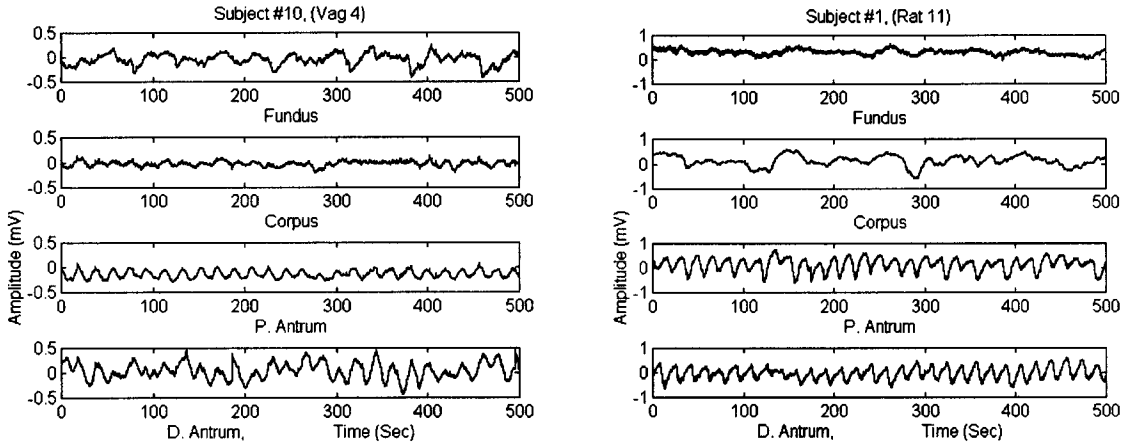

Figure 5.10: General Regional GEA Comparison

antrum recordings, which are very regular, consisting of a predominant slow wave component and a much more stable wave shape. This observation is illustrated in Figure 5.10. These data sets consist of the baseline recordings from the first atropine study and the fourth vagotomy study respectively. It is clear that the regularity of the slow wave varies between electrode locations.

There are several factors which may account for this regional difference. Anatomically, the circular muscle layer increases in thickness distally, being almost absent in the fundus. Thus, signals recorded from the fundus and orad corpus are comprised of longitudinal and oblique muscle activity which are suitable for tonic contraction and not phasic. It is reasonable to hypothesize that the predominant slow wave component, present in antral recordings, is mainly due to activity recorded from the circular muscle layer which undergoes phasic depolarization rings. The fundus recordings, on the other hand, are mainly due to different muscle layers which do not undergo these phasic depolarizations, and hence do not form regular, rhythmic slow wave activity. The inherent irregularity in these signals could be indicative of a less tight, directional coupling between muscle cells, leading to less regular signals due to uncoordinated propagation of plateau potentials throughout the syncytium of these muscle layers. This lack of coordinated propagation across the electrode site, results in the type of signal simulated in Figure 5.8. The difference in electrical activity between different muscle layers may be due to different intrinsic muscle properties, RMP, amount of gap junctions, concentration of ion channels, or may be due to differences in neural regulation. Differences between rats are due to many sources of variation, including differences in anatomy and slight differences in electrode position.

5.2.1 Signal Power Comparison

Recognizing that there are differences in underlying anatomy in different regions of the stomach, an attempt was made at quantifying the difference by quantifying the power of the slow wave component of the GEA recorded from each region. As expected, the observed signal power, quantified by signal variance of the 0.02 to 0.2 Hz bandwidth, generally increases distally. The mean variance from 10 recordings was observed to be 0.128 ± 0.041 in the fundus, 0.202 ± 0.070 in the corpus, 0.351 ± 0.147 in the proximal antrum and 0.422 ± 0.145 in the distal antrum, in nominal power units. A comparison is made between fundus and antral recordings in Figure 5.11. The fundus recordings, a, b and c, have a significantly smaller slow wave component than does the antral recording, d. As well, the significance of this differences

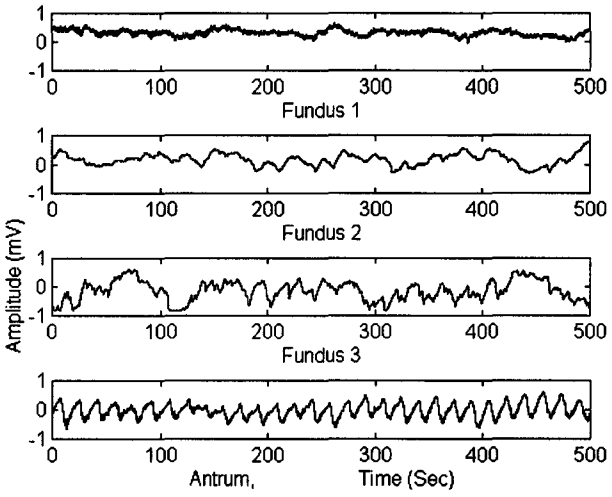

Figure 5.11: Fundic GEA, a, b & c are recordings from the distal fundus / proximal corpus, d, is a recording from the antrum for comparison

Subject	Fundus	Antrum
Rat # 1	0.0356	1.6317
Rat # 2	0.1035	0.10783
Rat # 3	0.4574	0.6239
Rat # 4	0.2072	0.15263
Rat # 5	0.0812	0.17128
Rat # 6	0.0314	0.21117
Rat # 7	0.0662	0.34222
Rat # 8	0.0594	0.25270
Rat # 9	0.0678	0.17029
Rat # 10	0.1728	0.55499
mean	0.1282	0.42187
stderr	0.0407	0.14525
mean, excl 1	0.1385	0.28744
sterr, excl 1	0.0440	0.06151
paired t-test, p		0.08211
t-test, excl 1, p		0.00999

Table 5.0: Slow Wave Power Comparison

* nominal units of power (variance)

is shown in Table 5.0, a comparison between fundus slow wave levels and antral levels. The results of a paired t-test shows that this trend is statistically significant with $p < 0.01$ after removal of a single outlier point.

The increase in signal level distally is consistent with an increase in circular muscle layer thickness distally. In the antrum, a thicker circular muscle layer results in more active muscle cells in close proximity to the recording electrode and a larger recorded slow wave component. Conversely, in the fundus, there is little or no circular muscle layer, speculated to be the source of the recorded rhythmic electrical activity, and hence a smaller amplitude of this slow wave. The plateau potentials are also known to be larger and longer in the antrum, also contributing to the increase in slow wave amplitude. Again, neural regulation may also be partially responsible for this observed difference, however this is uncertain. The relatively large, regular slow wave component of the antrum is a result of the lower RMP of muscle cells in this region, making them more suitable for phasic contractions and rhythmic electrical activity. Antral recordings are illustrated in Figure 5.12.

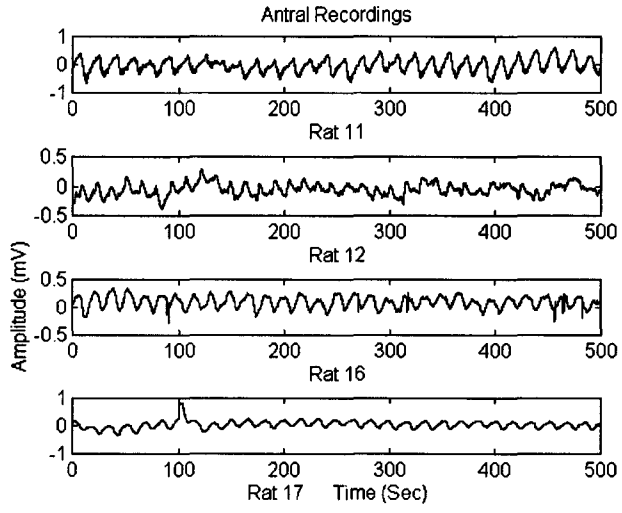

Figure 5.12: Antral Recordings of 4 Rats

5.2.2 Frequency Comparison

The power spectrum of each signal was calculated using both the periodogram method and the autoregressive method to determine the dominant slow wave frequency. The dominant frequency varied in the range of 0.047 Hz to 0.072 Hz with an average frequency of 0.054, calculated over all subjects and regions. There was found to be little

	Fundus	Corpus	P. Antrum	D. Antrum
1	0.0595	NA	0.0595	0.0595
2	NA	0.0717	0.0687	0.0717
3	NA	0.0534	0.0519	0.0534
4	0.0534	0.0534	0.0534	0.0534
5	NA	NA	0.061	0.0595
6	NA	NA	NA	0.0595
7	0.0488	0.0488	0.0488	0.0488
8	0.0488	0.0473	0.0473	0.0473
9	0.0504	0.0473	0.048	0.0488
10	0.058	0.0519	0.0519	0.0519

Table 5.1: Dominant Frequency Comparison

* values obtained from the periodogram estimate of dominant frequency

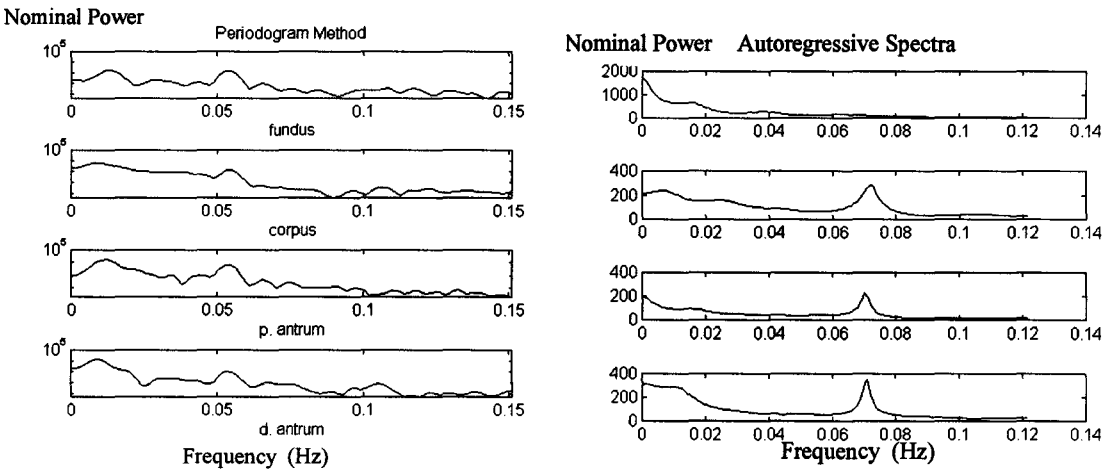

Figure 5.13: Comparison of Dominant Frequencies

* examples are for different subjects with dominant frequencies of 0.0519 and 0.0717 Hz respectively

* Δf for the periodogram method is 0.0015 Hz

or no variation between the baseline dominant frequency of different regions. Due to expected signal irregularity, for reasons discussed above, the dominant slow wave frequency was only calculable for a portion of the fundus recordings. However, it was very clear that no significant differences in frequency were present. Figures 5.13 and Table 5.1 illustrate these dominant frequencies.

5.3 Propagation Velocity

The velocity at which the rhythmic slow waves propagate distally can be determined by the time delay between slow wave peaks recorded at different electrodes. However, there are many factors which make this calculation very difficult. The differences in wave shapes and noise levels between electrodes, due to previously discussed factors, makes exact peak determination difficult. As well, the actual propagation velocity of an area may change over time. The estimates obtained are estimates of the average propagation velocity between the specific pair of electrodes. As well, they are averaged over time due to the methods used for calculation.

Several methods were examined and cross checked. The cross correlation function provides a determination of the lag which best represents the time delay between the two signals. Because of different wave shapes and inherent randomness of other components, this method provided only a moderately accurate estimate. The use of the cross spectrum provided another estimate [27]. The cross spectrum was used to determine the dominant frequency component, the slow wave component. Then the phase of the

cross spectrum, at the dominant frequency, was calculated to give the phase delay between the two electrodes. Finally, the estimated dominant frequency, the measured distance, and the calculated phase delay were used to give the actual propagation velocity. Figure 5.14 gives a sample calculation of the propagation based on a baseline atropine study data set.

We see from Figure 5.14 that the cross spectrum method seems to give an accurate estimate of the average propagation velocity. Due to this inherent lack of precision, these estimates are to be used only to get a feeling for the range of propagation velocities in a certain area. As is apparent, the fundus often completely lacks propagation of slow wave as discussed, and hence obviously cannot be calculated. The propagation velocities between the p. antrum and d. antrum were calculated for several data sets. These were found to be 0.3608, 0.1117, 0.1629, 0.2028 and 0.1326 cm / sec, slower than the range presented by Yamada, Tadataka [1], 0.5 to 4 cm / sec.

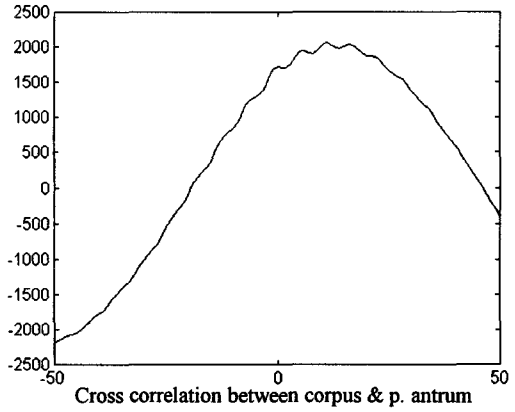

Cross correlation between corpus & p. antrum

* from cross correlation,
first peak at lag 13, therefore delay of 13/10 = 1.3 seconds

* from cross spectrum,
dominant frequency = 0.0708
phase delay @ 0.0708 Hz = -0.861 rad
therefore, time delay = -0.861 / (2π*0.0708) = 1.94 seconds

* from actual signal,
by examining 3rd slow wave
corpus = 2940, p.antrum = 3125, difference = 185
therefore, time delay = 1.85 seconds

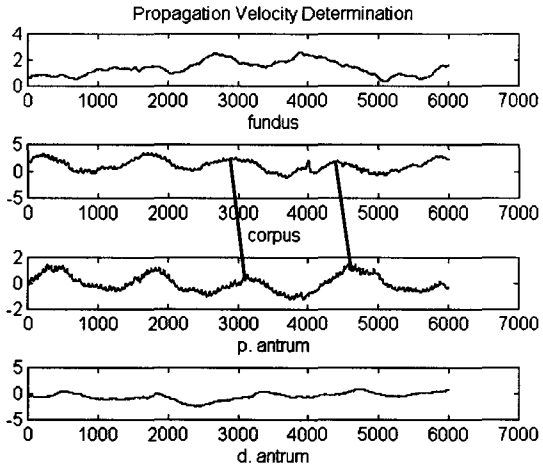

* time scale = sample number, fs = 100 samples per second, amplitude scale = volts with gain factor of 6K

Propagation Velocity

from cross correlation = 0.7 / 1.3 = 0.5385 cm per second
from cross spectrum = 0.7 / 1.94 = 0.3608 cm per second
from visual estimation = 0.7 / 1.85 = 0.3784 cm per second

Figure 5.14: Propagation Velocity Determination

Chapter 6

Neural Control of Gastric Electrical Activity

6.0 Neural Pathways and Reflexes

There are many different neural pathways through which control information is passed to the regions of the stomach. These pathways involve enteric neurons, autonomic neurons, and neurons of the brainstem. Local pathways such as from the effector cells to enteric neurons and back again, control local mechanisms such as local secretion and muscle tone. As well, more global pathways exist which act as a global control system, adjusting function of the stomach to suit the requirements of the gastrointestinal tract and the body as a whole. Information from different sections of the gastrointestinal tract is fed back through different neural pathways to effect the function of other sections.

These control mechanisms between different regions are termed reflexes. Several gastrointestinal system reflexes have been identified and are widely accepted today. The relaxation reflex uses information from the esophagus, through global feedback pathways, to relax gastric tone by way of non-adrenergic non-cholinergic neurons (NANC). Another reflex is the accommodation reflex, which maintains gastric pressure by relaxing gastric tone upon distention of the stomach. This reflex is a tight local reflex using local information about the state of the stomach to control the stomach. The enterofundic

reflex involves relaxation of fundic tone based on fat, protein and sugar content and distention of the small bowel. Antral peristalsis, a factor contributing to gastric emptying, is stimulated by distention of the stomach. This reflex, known as the antral reflex, increases antral peristalsis, the movement of chyme towards the pylorus, in response to filling of the stomach. On the other side of this control mechanism is the enterogastric reflex, which inhibits antral peristalsis due to distention in the small bowel. Finally, there are the pyloric and gastroenteric reflexes which control the state of the pylorus, a flow control valve, based on acid in the small bowel mucosa and gastric distention respectively. This brief introduction to gastrointestinal reflexes illustrates the integration of system information and control system at several levels, which is responsible for proper function of the digestive system.

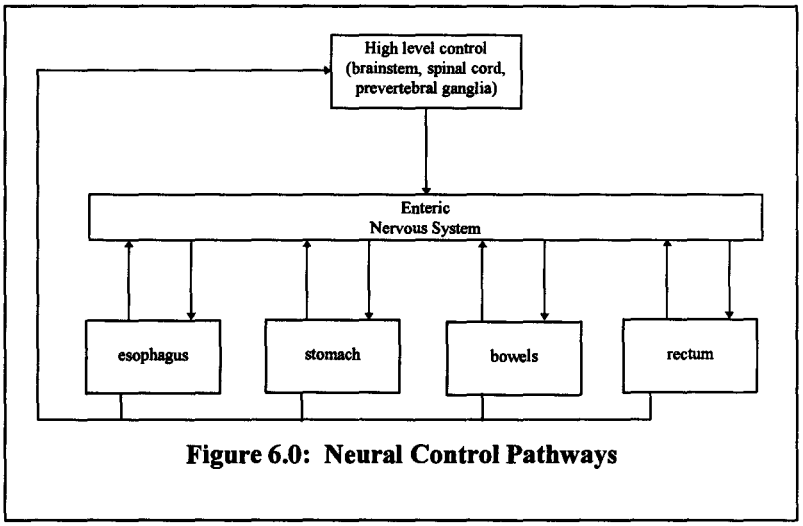

Figure 6.0: Neural Control Pathways

6.1 Summary of Factors Effecting Normal Gastric Electrical Activity

Many factors have been shown to be involved with the normal rhythmic electrical activity of the stomach. Interstitial cells of Cajal, coupling through gap junctions, innervation and neurotransmitter release, gated ion channels, hormones, and many other

factors make up the complex mechanism responsible for the observed characteristics of GEA. No attempt will be made to definitively explain the physiological basis responsible for observed changes in recordings, but rather, only a discussion will be presented of the possible mechanisms, with reference to known aspects of physiology.

As a front of cell membrane depolarization waves propagate from muscle cell to muscle cell longitudinally down the muscle syncytium, it passes the electrode recording location creating an integrated "slow wave" signal. However, this process is very complex leading to several important questions. Where does this propagating wave originate? What is responsible for generating this wave? What resulting functionality is this electrical activity responsible for? How does this wave propagate along the syncytium? What factors and mechanisms control this activity and generate a normally functioning stomach? These questions, among many, have motivated this work.

It has become widely accepted by many researchers, that this electrical activity is responsible for the highly organized muscle contractions of the gastrointestinal tract [1,2]. The tonic contractions of the fundus, the strong phasic, peristaltic contractions in the antrum, and the contraction of the pyloric sphincter, are all precisely controlled by this electrical activity. Thus, the control mechanisms of GEA are also control mechanisms for contraction and functionality of the stomach.

Although there is still uncertainty as to the exact source of the rhythmic fluctuation of the membrane potential in the smooth muscle cells, it has been shown that Interstitial Cells of Cajal play a key role. It is believed that these "pacemaker" cells have

an intrinsic rhythmicity in their membrane potential, which is transferred to the smooth muscle by some means. Thus, without interstitial cells, smooth muscle cells would be devoid of slow waves [3]. It is thought that interstitial cells, located between the circular and longitudinal muscle layers throughout the stomach, have a prominent effect in the orad corpus, where the propagating slow waves are believed to originate [1,4]. A distally decreasing frequency gradient in the electrical rhythmicity is theorized to be responsible for this site of origin. The fast frequency of rhythmicity in this area and the electrical coupling between cells in the syncytium force more distal cells to this frequency by the propagating wave [1,16]. This has been termed entrainment [16].

This slow wave is believed to propagate circumferentially in the circular muscle, and distally in the longitudinal muscle [17]. The circular muscle layer is known to be rich in gap junctions in the circumferential direction. Thus, tight electrical coupling between cells propagates the membrane depolarization very quickly around the circumference of the stomach. The longitudinal muscle layer, however, is known to contain few, if any, gap junctions, and thus propagation in the longitudinal direction might rely on some other, slower mechanism. These properties make sense since the result would be a circular ring of depolarization and hence contraction, which is propagated distally at a much slower rate.

It is also known that neural control plays a key role in mediating this electrical activity. In this way, the gastric electrical activity , contraction of smooth muscle, and hence functionality of the stomach may be altered in response to various factors and

gastrointestinal tract states, through reflex pathways. Exactly how neurons exert control over this electrical activity is uncertain. Information about the state of all regions of the gastrointestinal tract is sent via afferent nerves to control centers, at different levels of the system. Locally in the myenteric and submucosal plexi, or globally in the spinal cord and brain stem, this information is processed and afferent information sent back to control different aspects of the stomach. This may be done by precisely controlled neurotransmitter release. The neurotransmitters may alter GEA by opening or closing excitatory or inhibitory ion channels, thus raising or lowering the membrane potential of the innervated muscle cell. Although the mechanism for how the neurons alter the slow waves and hence gastric function is uncertain, it is clear that they are essential for normal function.

6.2 Response To Stimuli

The process of identifying the mechanisms of a control system require the observation of responses to disturbances in the state of the process. By altering the state of the nervous control of the stomach, through the use of various forms of stimuli, and observing the accompanying changes in GEA, we are able to break down the control system and determine its functionality. This type of control system identification is performed in many fields of engineering by well developed methods[15]. Due to its size, complexity and applicability, the gastric neural control system of the rat was examined with several stimuli, however not in sufficient detail to obtain a parametric model for the

entire control system. Statistical techniques were applied to analyze the observed responses and clearly show significant trends in the presence of many sources of error and variation.

Several signal characteristics were compared between recordings using the processing techniques presented in chapter 4. The characteristics of the dominant slow wave, very important features of GEA, were examined for power and frequency changes. The dominant frequency of the slow wave, defined here by the most predominant spectral peak in the slow wave frequency range of 0.02 Hz to 0.08 Hz, was determined subjectively by examination of the estimated power spectrum. However it should be noted that in areas without predominant slow wave activity, such as in several fundic recordings, there may not be a dominant slow wave frequency. The power of the slow wave was quantified by the variance of the recorded GEA, bandlimited to the range of 0.02 Hz to 0.2 Hz. In order to determine if changes in slow wave variance reflect decreases in power or if the slow wave simply shifted its power to much lower frequencies, an alternative means of estimating signal power was calculated for the recorded GEA. The power spectrum estimate for each signal was integrated for the range 0 Hz to 0.1 Hz. A lower upper bound of 0.1 Hz was used as a tighter isolation of the slow wave frequency range and possible lower frequencies. Finally, short term fluctuations in dominant frequency, possibly representing neural modulation, were examined by examining time - frequency estimates.

6.2.0 Atropine

Atropine was given intramuscularly to anesthetized Sprague-Dawley rats in accumulated doses as outlined in standard procedure B.0 in appendix B. Atropine is a competitive muscarinic cholinergic receptor antagonist [8]. Atropine competes with acetylcholine for receptor sites on the smooth muscle cells, thus causing a decrease in the communication between nerve terminals and the smooth muscle cells. At the system level, we can conclude that atropine effectively breaks, or at least significantly diminishes, muscarinic cholinergic neural connections. As mentioned previously, it is believed that excitatory enteric neurons communicate with gastric smooth muscle cells via the neurotransmitter acetylcholine. Thus doses of atropine should reduce the number of excitatory neurons connected to the smooth muscle syncytium. Figure 6.1 illustrates a sample data set recorded at accumulated doses of atropine.

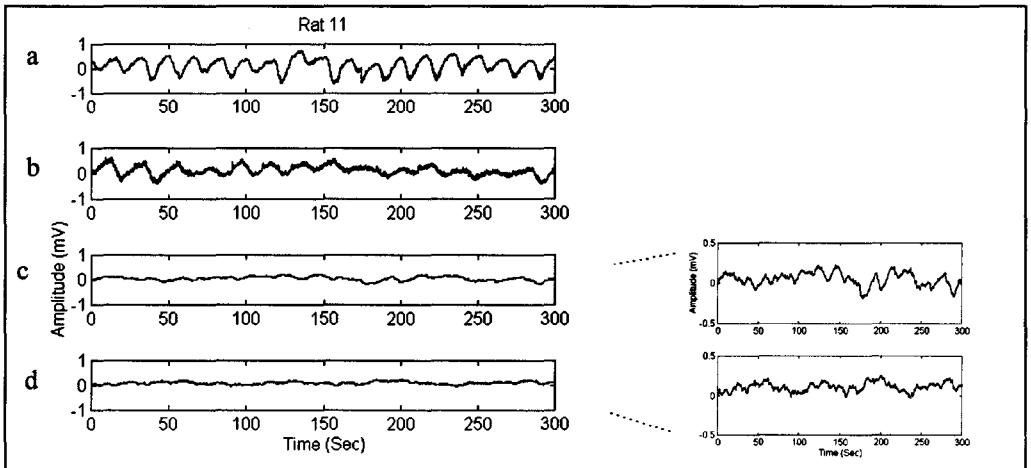

Figure 6.1: Sample Accumulated Atropine Data Set (antrum)

a) baseline b) 1st dose c) 2nd dose d) 3rd dose

6.2.0.0 Results

The results of 6 sets of atropine injection recorded data, for six rats studied, are illustrated in Table 6.0, variance comparison; Table 6.1, frequency comparison; and Table 6.2, signal power comparison in nominal units, as alternatively calculated by integration of power spectra. The unbiased sample signal variance, defined as: $\frac{1}{n-1}\sum_{k=1}^{n}(y_k - \bar{y})^2$, is calculated for each 20 minute recorded signal to estimate signal power. Variance values are given as computed from amplified signals, amplified by 6 000 times. Therefore a conversion factor of 6000^2 ($3.6\text{x}10^7$) relates this value to power of source signal in V^2. Table 6.0 contains the recorded variance value of each signal, organized into 6 subjects (rows) for each separate region at the 4 experimental points (columns). The variance is then averaged over all 6 subjects and a standard error of this average is calculated, for each region. Next, the change in variance is normalized by expressing it as a percentage change from the baseline variance. A paired t-test was performed to test for significance between baseline and final atropine dose. For the raw variance data, no significant difference was observed. However for the normalized data, the antrum results were significantly different. As well, a few outlier points were excluded, showing definite significance at all recording locations. These points were excluded on the basis that they represent data sets with a relatively small baseline variance value. This could indicate that, for practical reasons, the amount of actual GEA recorded by this channel is very low. Therefore changes in signal variance may not represent changes in GEA, but rather,

changes in noise and artifact levels. Given that the changes in variance are normalized to percentage change from baseline variance, these points have a very profound effect on the level of significance of trend and are justified to be excluded.

Table 6.1 lists the dominant slow wave frequency, calculated with the periodogram method, for each subject at each location (row) and experimental point (column). Some recordings showed no dominant frequency, due to recording conditions or simply lack of slow wave activity in that region, most namely, the fundus. For this reason, some dominant frequencies in Table 6.1 are disregarded. Since it has been previously observed that there is little or no variation in dominant frequency between electrode locations and we are interested only in the effect of atropine on dominant frequency, the values for each location are averaged for each rat at each experimental point. A paired t-test is performed between baseline dominant frequency and dominant frequency after final atropine dose to illustrate the significance of the observed trend.

Table 6.2 (a), which is organized as in Table 6.0, lists values for each subject at each location and experimental point representing signal power by the integral of the estimated power spectrum from 0 Hz to 0.1 Hz. These values are also shown, in Table 5.2 (b), organized by electrode location, and normalized, in Table 5.2 (c), as a percentage change from baseline. Paired t-tests are performed and outlier points, the same as in Table 6.0, are removed.

The results of Table 6.0 clearly show a significant decrease in slow wave power with increasing doses of atropine. After removal of outliers, average percentage decreases from baseline of -67.9 ± 18.0, -83.1 ± 9.8, -66.5 ± 11.5, and -60.6 ± 10.9 were calculated for the fundus, corpus, p. antrum and d. antrum respectively This trend was shown to be significant with $p < 0.05$ for all regions. It can also be concluded, from Table 6.1, that atropine causes a decrease in dominant slow wave frequency, although only slight. A paired t-test estimates that there is only about a 6% probability of the trend only being due to chance, close to accepted significance. Figure 6.2 shows an example of this slow wave frequency decrease. There are approximately 18 slow waves in 5 minutes of baseline recording, a frequency of 3.6 cpm or 0.06 Hz. This is lowered at final dose to only 15 slow waves in 5 minutes or a frequency of 3.0 cpm or 0.05 Hz. This is a very suitable example since calculated averages are 0.0594 Hz at baseline and 0.0509 Hz at final dose. Signal power, as calculated from the power spectra over the range 0 to 0.1 Hz, is likewise decreased by atropine, confirming by a second

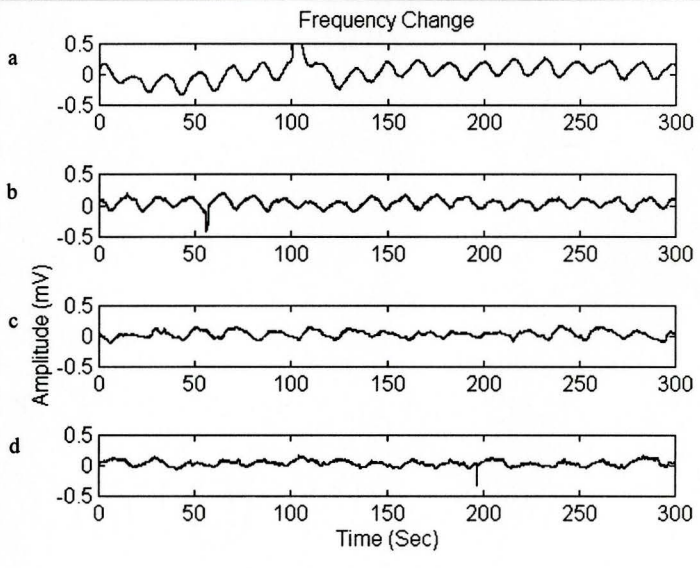

Figure 6.2: Frequency Change With Increasing Atropine Dose
a) baseline b) 1st dose C) 2nd dose d) 3rd dose

quantification of signal power, the effect of atropine on signal power levels. Average percentage decreases from baseline of -71.2 ±16.8, -76.5 ± 8.7, -59.8 ± 20.8 and -48.9 ± 15.2, respectively in the fundus, corpus, p. antrum and d. antrum, are illustrated in Table 6.2. It is concluded that a decrease in power of 64.1% on average by power spectra corresponds well with the decrease in slow wave variance, another measure of signal power, of 69.5 % on average. The difference possibly being attributed to differences in signal bandwidths. Thus, although there is a slight frequency shift, the power decrease is not due to a shift in dominant frequency components out of the assumed slow wave range. It should be noted that the small number of subjects, n = 6 and n = 4 with outliers normally results in lower levels of significance. Thus the trends illustrated here are quite significant trends.

Table 6.0: Changes in Bandlimited Signal (0.02 - 0.2) Variance With Atropine Doses

Atropine Variance Results

	without normalization						percentage change from average baseline					outliers removed	
	baseline	atropine1	atropine2	atropine3	t-test		base perc	atropine1	atropine2	atropine3	t-test	atropine3	t-test
	fundus						fundus						
1	0.0356	0.0459	0.0387	0.0435		1	0	28.9055	8.5126	22.1703			
2	0.1035	0.0473	0.0372	0.0186		2	0	-54.2673	-64.0902	-81.9968		-81.9968	
3	0.4574	0.7162	0.0680	0.0249		3	0	56.5807	-85.1334	-94.5489		-94.5489	
4	0.2073	0.3509	0.3448	0.3429		4	0	69.2827	66.3718	65.4390			
5	0.0812	0.0315	0.0125	0.0159		5	0	-61.1684	-84.6548	-80.3866		-80.3866	
6	0.0315	0.0156	0.0323	0.0268	0.388565	6	0	-50.4251	2.5728	-14.7488	0.3034	-14.7488	0.0326
mean	0.1527	0.2012	0.0889	0.0788		mean	0	-1.8486	-26.0702	-30.6786		-67.9203	
stderr	0.0663	0.1153	0.0517	0.0530		stderr	0	24.5260	25.1184	26.7515		18.0043	
	corpus						corpus						
1	0.0875	0.0314	0.0167	0.0090		1	0	-64.1280	-80.8835	-89.7563		-89.7563	
2	0.7391	0.6560	0.0787	0.0495		2	0	-11.2479	-89.3519	-93.3072		-93.3072	
3	0.3159	0.0939	0.0260	0.0247		3	0	-70.2754	-91.7695	-92.1916		-92.1916	
4	0.2107	0.2821	0.1898	0.1178		4	0	33.8924	-9.8892	-44.0665		-44.0665	
5	0.0282	0.0728	0.0902	0.0835		5	0	158.4136	220.0114	196.2888			
6	0.1084	0.0137	0.0049	0.0042	0.122439	6	0	-87.3324	-95.4490	-96.1466	0.4744	-96.1466	0.0011
mean	0.2483	0.1916	0.0677	0.0481		mean	0	-6.7796	-24.5553	-36.5299		-83.0936	
stderr	0.1066	0.1008	0.0282	0.0184		stderr	0	37.7590	50.6436	47.2477		9.8107	
	p.antrum						p.antrum						
1	1.5234	0.4021	0.0429	0.0215		1	0	-73.6079	-97.1862	-98.5865		-98.5865	
2	0.2059	0.0911	0.0631	0.0729		2	0	-55.7552	-69.3379	-64.6107		-64.6107	
3	0.2739	0.1475	0.0686	0.0441		3	0	-46.1417	-74.9391	-83.8851		-83.8851	
4	0.7882	0.4767	0.2187	0.1333		4	0	-39.5204	-72.2490	-83.0838		-83.0838	
5	0.0780	0.0808	0.0406	0.0604		5	0	3.5611	-47.9778	-22.6148		-22.6148	
6	0.0624	0.0064	0.0137	0.0335	0.128617	6	0	-89.6612	-78.0010	-46.2278	0.0022	-46.2278	0.0022
mean	0.4886	0.2008	0.0746	0.0610		mean	0	-50.1876	-73.2818	-66.5014		-66.5014	
stderr	0.2336	0.0782	0.0299	0.0163		stderr	0	13.1108	6.4636	11.4706		11.4706	
	d.antrum						d.antrum						
1	1.6317	0.1171	0.1239	0.0764		1	0	-92.8255	-92.4046	-95.3198		-95.3198	
2	0.1078	0.0715	0.1217	0.0551		2	0	-33.6940	12.8594	-48.9335		-48.9335	
3	0.6239	0.4697	1.0036	0.2534		3	0	-24.7155	60.8591	-59.3845		-59.3845	
4	0.1526	0.2236	0.1876	0.1251		4	0	46.5167	22.9089	-18.0389		-18.0389	
5	0.1713	0.1670	0.0681	0.0677		5	0	-2.4763	-60.2179	-60.4829		-60.4829	
6	0.2112	0.0124	0.0627	0.0394	0.174438	6	0	-94.1394	-70.2906	-81.3214	0.0026	-81.3214	0.0026
mean	0.4831	0.1769	0.2613	0.1028		mean	0	-33.5557	-21.0476	-60.5802		-60.5802	
stderr	0.2422	0.0658	0.1496	0.0324		stderr	0	22.0900	25.0610	10.9299		10.9299	

* variance values calculated from recorded units with a gain of 6000
convert to source units by division by factor of 6000 squared = 36000000, leaving variance units of V squared.

Table 6.1: Changes in Dominant Slow Wave Frequency With Atropine Doses

Atropine Frequency Results

		baseline	atropine1	atropine2	atropine3
rat 11	fundus	0.0595			
	corpus				
	p.antrum	0.0595	0.0458	0.0443	
	d.antrum	0.0595	0.0488		
mean		0.0595	0.0473	0.0443	
rat 12	fundus		0.0565	0.0534	0.0519
	corpus	0.0717	0.0565	0.0504	0.0488
	p.antrum	0.0687	0.0626	0.0534	0.0534
	d.antrum	0.0717	0.0595	0.0549	0.0519
mean		0.0707	0.0588	0.0530	0.0515
rat 14	fundus		0.0488	0.0549	0.0580
	corpus	0.0534	0.0443	0.0565	0.0580
	p.antrum	0.0519	0.0488	0.0549	0.0580
	d.antrum	0.0534	0.0488	0.0549	0.0580
mean		0.0529	0.0477	0.0553	0.0580
rat 15	fundus	0.0534	0.0519	0.0504	0.0488
	corpus	0.0534	0.0519	0.0504	0.0504
	p.antrum	0.0534	0.0519	0.0504	0.0519
	d.antrum	0.0534	0.0504	0.0488	0.0488
mean		0.0534	0.0515	0.0500	0.0500
rat 16	fundus		0.0519	0.0473	0.0488
	corpus		0.0519	0.0488	0.0504
	p.antrum	0.0610	0.0519	0.0488	0.0519
	d.antrum	0.0595	0.0519	0.0488	0.0488
mean		0.0603	0.0519	0.0484	0.0500
rat 17	fundus		0.0626	0.0595	0.0519
	corpus		0.0626		0.0519
	p.antrum		0.0626	0.0595	0.0519
	d.antrum	0.0595	0.0626	0.0595	0.0519
mean		0.0595	0.0626	0.0595	0.0519

	baseline	atropine1	atropine2	atropine3	t-test
rat 11	0.0595	0.0473	0.0443	0.0443	
rat 12	0.0707	0.0588	0.0530	0.0515	
rat 14	0.0529	0.0477	0.0553	0.0580	
rat 15	0.0534	0.0515	0.0500	0.0500	
rat 16	0.0603	0.0519	0.0484	0.0500	
rat 17	0.0595	0.0626	0.0595	0.0519	
mean	0.0594	0.0533	0.0518	0.0509	0.0625

delta f = 0.0015 Hz

Atropine Power Results (from integration of PSD over 0 to 0.1 Hz)

a) by subject

	baseline1	atropine1	atropine2	atropine3
rat 11	11629	29255	33252	
	49438	22369	5047	
	81360	33566	9798	
	66409	67641	11948	
	52209	38208	15011	
rat 12	58516	16371	24861	10787
	76747	76357	29040	20403
	12341	11944	11772	6625
	13869	8301	14608	16841
	40368	28243	20070	13664
rat 14	131210	198580	43909	13083
	23475	13207	3665	3228
	28841	12300	7523	5970
	42451	31377	55640	22309
	56494	63866	27684	11148
rat 15	18585	17952	27258	71784
	70776	15720	16026	39853
	144150	71101	64407	21982
	79653	28977	20546	38256
	78291	33438	32059	42969
rat 16	42109	16133	19071	3440
	3024	11514	27116	11010
	6802	15618	27422	9383
	9603	6341	8901	4234
	15385	12402	20628	7017
rat 17	6597	1742	1216	5194
	17031	1241	6351	1835
	122010	1255	1106	2099
	13949	5930	557	3119
	39897	2542	2308	3062

b) by region

	baseline1	atropine1	atropine2	atropine3
fundus	11629	29255	33252	
	58516	16371	24861	10787
	131210	198580	43909	13083
	18585	17952	27258	71784
	42109	16133	19071	3440
	6597	1742	1216	5194
	44774	46672	24928	20858
	19069	30591	5864	12853
corpus	49438	22369	5047	
	76747	76357	29040	20403
	23475	13207	3665	3228
	70776	15720	16026	39853
	3024	11514	27116	11010
	17031	1241	6351	1835
	40082	23401	14541	15266
	12321	10955	4641	6980
p. antrum	81360	33566	9798	
	12341	11944	11772	6625
	28841	12300	7523	5970
	144150	71101	64407	21982
	6802	15618	27422	9383
	122010	1255	1106	2099
	65917	24297	20338	9212
	23976	10295	9506	3398
d. antrum	66409	67641	11948	
	13869	8301	14608	16841
	42451	31377	55640	22309
	79653	28977	20546	38256
	9603	6341	8901	4234
	13949	5930	557	3119
	37656	24761	18700	16952
	12286	9773	7864	6464

c) by region (normalized to percentage change from baseline)

baseline1	atropine1	atropine2	atropine3	t-test	no outliers	t-test
0.0000	151.5694	185.9403	185.9403			
0.0000	-72.0230	-57.5142	-81.5657		-81.5657	
0.0000	51.3452	-66.5353	-90.0290		-90.0290	
0.0000	-3.4060	46.6667	286.2470			
0.0000	-61.6875	-54.7104	-91.8307		-91.8307	
0.0000	-73.5941	-81.5674	-21.2672	0.6601	-21.2672	0.0240
0.0000	-1.2993	-4.6200	31.2491		-71.1732	
0.0000	36.5239	42.4283	66.9068		16.7851	
0.0000	-54.7534	-89.7913	-89.7913		-89.7913	
0.0000	-0.5082	-62.1614	-73.4152		-73.4152	
0.0000	-43.7401	-84.3876	-86.2492		-86.2492	
0.0000	-77.7891	-77.3567	-43.6914		-43.6914	
0.0000	280.7540	796.6931	264.0873			
0.0000	-92.7133	-62.7092	-89.2255	0.7444	-89.2255	0.0009
0.0000	1.8750	70.0478	-19.7142		-76.4745	
0.0000	57.2596	145.4011	57.2048		8.7165	
0.0000	-58.7439	-87.9572	-87.9572		-87.9572	
0.0000	-3.2169	-4.6106	-46.3172		-46.3172	
0.0000	-57.3524	-73.9156	-79.3003		-79.3003	
0.0000	-50.6757	-55.3195	-84.7506		-84.7506	
0.0000	129.6089	303.1461	37.9447		37.9447	
0.0000	-98.9714	-99.0935	-98.2796	0.0350	-98.2796	0.0350
0.0000	-23.2252	-2.9584	-59.7767		-59.7767	
0.0000	33.0030	62.7020	20.8264		20.8264	
0.0000	1.8552	-82.0085	-82.0085		-82.0085	
0.0000	-40.1471	5.3284	21.4291		21.4291	
0.0000	-26.0865	31.0688	-47.4476		-47.4476	
0.0000	-63.6210	-74.2056	-51.9717		-51.9717	
0.0000	-33.9686	-7.3102	-55.9096		-55.9096	
0.0000	-57.4880	-96.0069	-77.6400	0.0235	-77.6400	0.0235
0.0000	-36.5760	-37.1890	-48.9247		-48.9247	
0.0000	9.6182	21.7548	15.1976		15.1976	

* results given in nominal units from numerical integration of discrete power spectrum for 0 to 0.1 Hz.

Table 6.2: Changes in Signal Power With Atropine Doses

6.2.0.1 Discussion

It has been concluded that signal power and slow wave frequency are decreased by atropine. These results make intuitive sense since atropine blocks muscurinic cholinergic nerve transmission, known to be excitatory. However, exactly why this results in less signal power and a lower dominant frequency is uncertain. It may be speculated that the removal of the basic firing patterns of excitatory neurons, causes changes in the recorded slow wave. The membrane potential may be lowered in some highly innervated muscle cells, to a point where, even with stimulation from other active muscle cells and interstitial cells, the membrane potential never exceeds the threshold for the occurrence of a membrane depolarization wave. If this indeed were the case, fewer muscle cells would undergo depolarization waves and thus the recorded slow wave would consist of an integration of contribution from fewer muscle cells. Hence, the recorded slow wave would be smaller. Although no evidence of this mechanism exists, its results are consistent with recorded slow wave power changes.

Many believe that the higher frequency at the site of origin of the propagating slow wave entrains distal muscle cells to this frequency. Thus, if the site of origin is moved to cells with a slightly slower intrinsic frequency, the frequency of the propagating slow wave would also decrease. This could possibly happen as a result of decrease of excitatory neural stimulation in this area. This is a possible, consistent explanation for the observed change. Although atropine blocks many excitatory neurotransmitters. It is

believed that other excitatory neurotransmitters are also involved, to a lesser extent. This fact accounts for the variance decreasing 69.5 percent on average, an incomplete inhibition of slow wave activity. Whatever the exact mechanism, it is clear from these recordings that atropine did have a significant effect on slow waves, suggesting that intrinsic neurons do mediate gastric electrical activity.

The neural mediation of GEA has clearly been shown as an important part of the gastric control mechanism. However, due to its complexity, the decrease in slow wave activity may not completely reflect the effects of atropine. The decrease in muscarinic cholinergic excitatory neural input may be accompanied by compensatory mechanisms. These changes, through neural feedback pathways or other routes, may alter inhibitory neural input or possibly excitatory neural input which uses neurotransmitters other than acetylcholine. Other factors, such as chemical and hormonal responses, may also play significant roles. Thus, the only certain conclusion is that gastric neural input does indeed effect the generation of gastric electrical activity, which in turn plays a role in control of gastric motility.

Finally, it should be mentioned that the effects of atropine are not selective to gastric innervation. Other physiological effects accompany the effect on the stomach. These include, increased heart rate, reduced mucous secretions, decreased bronchial resistance, and inhibition of sweating [8]. These physiological effects may effect the physiological state of the gastrointestinal tract and indirectly contributed to the observed changes in GEA.

6.2.1 Vagotomy

A full truncal vagotomy was performed to effectively remove parasympathetic nerve control effects on the rest of the system. Thus, a major feedback pathway was removed. The standard procedure outlined in B.1 in appendix B, was performed on 4 rats. Although the vagus trunks are sectioned before branching occurs, anatomical features vary slightly between subjects and it is possible that some branches were missed. However, the majority of the stomach can be assumed to be devoid of vagal control. The two vagal trunks, anterior and posterior, were sectioned in random order to investigate any anatomical dependence that GEA may have on vagal innervation.

6.2.1.0 Results

The results of 4 sets of vagotomy experiment recordings, from 4 different rats, are illustrated in Table 6.3, slow wave variance changes; Table 6.4, dominant frequency changes; and Table 6.5, signal power changes over 0 to 0.1 Hz, again estimated by the integration of the periodogram power spectral estimates. The results are organized in a similar fashion to the atropine study results. However, two separate baseline recordings were taken and an average of the two is used for calculations of percent change. Also, in Table 6.4, t-test values are given for the significance of decrease from baseline to first vagotomy, from baseline to second vagotomy and from baseline to average vagotomy, where average vagotomy is simply the mean of the two previous results. The average was

used because the results show that there is a significant decrease from baseline to first vagotomy, but not from one randomly chosen sectioned vagus trunk to full truncal vagotomy.

Vagotomy clearly reduces slow wave amplitude and power. Table 6.3 illustrates this trend with percentage decreases from baseline of -44.6 ± 13.3, -42.3 ± 22.4, -47.9 ± 10.5, and -35.8 ± 11.6, in the fundus, corpus, p. antrum, and d. antrum regions respectively, after full vagotomy. This trend is almost at an accepted significance level in all regions, with p = 0.078 in the fundus, p = 0.200 in the corpus, p = 0.020 in the p. antrum and p = 0.054 in the d. antrum. The significance of these results is high considering that only 4 data sets are available, with only 3 when outliers are removed from the fundus and corpus results. The most significant trend seems to be after only one trunk is removed, with percentage decreases from baseline of -32.7 ± 10.7, p = 0.055, -37.9 ± 25.2, p = 0.229, -56.6 ± 9.0, p = 0.008, and -43.9 ± 17.0, p = 0.081, in the fundus, corpus, p. antrum and d. antrum respectively. It seems that there is little or no difference between a single sectioned vagal trunk and full

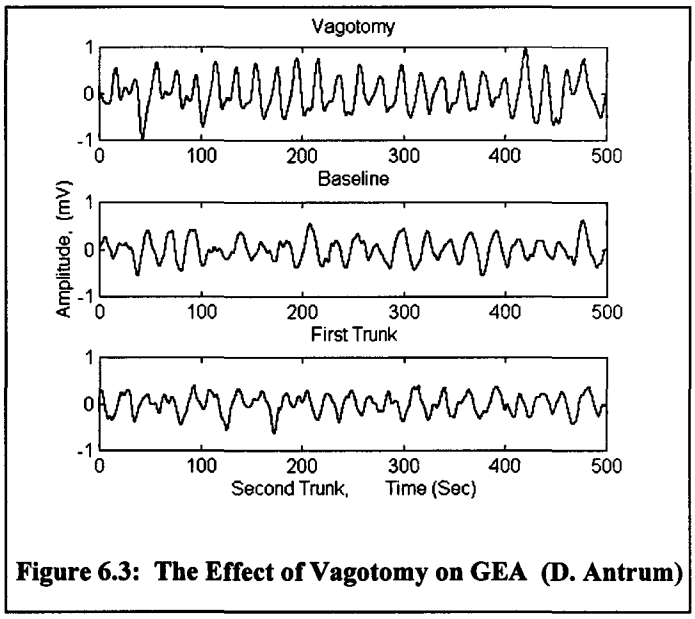

Figure 6.3: The Effect of Vagotomy on GEA (D. Antrum)

vagotomy. Table 6.4 illustrates that, as well, there is no significant frequency change associated with vagotomy. Finally, similar changes in signal power, from the power spectra quantification, are listed in Table 6.5, with percentage decreases of -35.9 ± 9.7, -37.7 ± 9.6, -51.5 ± 14.4, and -40.1 ± 15.7, respectively in the fundus, corpus, p. antrum, and d. antrum. Again the decrease in signal power of 41.3 % on average, from power spectra, corresponds well with the decrease in slow wave variance, another measure of signal power, of 42.6 % on average. Figure 6.3 illustrates the above conclusions regarding the effects of vagotomy on GEA.

Table 6.3: Changes in Bandlimited Signal (0.02 - 0.2) Variance With Truncal Vagotomy

Vagus Variance Results

	without normalization						percentage change from average baseline					outliers removed	
	baseline1	baseline2	1st trunk	2nd trunk	t-test	avg base		base perc	1st trunk	2nd trunk	t-test	2nd trunk	t-test
	fundus							fundus					
1	0.0663	0.0837	0.0421	0.0246		0.0750	1	0	-43.8873	-67.1352		-67.1352	
2	0.0595	0.0823	0.0560	0.0855		0.0709	2	0	-21.0203	20.5280			
3	0.0678	0.0611	0.0583	0.0508		0.0645	3	0	-9.5209	-21.1430		-21.1430	
4	0.1728	0.0749	0.0538	0.0673	0.2096	0.1239	4	0	-56.5329	-45.6558	0.2288	-45.6558	0.0783
mean	0.0916	0.0755	0.0526	0.0571			mean	0	-32.7403	-28.3515		-44.6447	
stderr	0.0271	0.0052	0.0036	0.0129			stderr	0	10.6726	18.8078		13.2864	
	corpus												
1	0.0412	0.0708	0.0763	0.0652		0.0560	1	0	36.1777	16.4128			
2	0.0875	0.0797	0.0349	0.0735		0.0836	2	0	-58.2933	-12.0712		-12.0712	
3	0.3503	0.5442	0.1074	0.0627		0.4473	3	0	-75.9828	-85.9741		-85.9741	
4	0.0485	0.1197	0.0391	0.0599	0.3570	0.0841	4	0	-53.5394	-28.7109	0.2910	-28.7109	0.1997
mean	0.1319	0.2036	0.0644	0.0653			mean	0	-37.9094	-27.5859		-42.2521	
stderr	0.0735	0.1140	0.0171	0.0029			stderr	0	25.1633	21.5775		22.3825	
	p.antrum												
1	0.1048	0.1386	0.0288	0.0262		0.1217	1	0	-76.3782	-78.4616		-78.4616	
2	0.2260	0.1093	0.0667	0.1075		0.1677	2	0	-60.2386	-35.8646		-35.8646	
3	0.0760	0.1627	0.0804	0.0657		0.1194	3	0	-32.6881	-44.9288		-44.9288	
4	0.1692	0.2496	0.0901	0.1416	0.0049	0.2094	4	0	-56.9610	-32.3925	0.0198	-32.3925	0.0198
mean	0.1440	0.1651	0.0665	0.0853			mean	0	-56.5665	-47.9118		-47.9118	
stderr	0.0336	0.0302	0.0135	0.0251			stderr	0	9.0200	10.5205		10.5205	
	d.antrum												
1	0.3422	0.4175	0.1935	0.1838		0.3799	1	0	-49.0493	-51.6223		-51.6223	
2	0.2527	0.1003	0.0537	0.1001		0.1765	2	0	-69.5918	-43.2932		-43.2932	
3	0.1703	0.2628	0.2281	0.2134		0.2166	3	0	5.3356	-1.4748		-1.4748	
4	0.5550	0.8646	0.2675	0.3781	0.1253	0.7098	4	0	-62.3209	-46.7349	0.0535	-46.7349	0.0535
mean	0.3301	0.4113	0.1857	0.2188			mean	0	-43.9066	-35.7813		-35.7813	
stderr	0.0828	0.1644	0.0465	0.0583			stderr	0	16.9560	11.5624		11.5624	

* units as in Table 6.0

Table 6.4: Changes in Dominant Slow Wave Frequency With Vagotomy

Vagotomy Frequency Results

by subject

	baseline1	baseline2	avg base	trunk1	trunk2	avg trunk
vag1	0.0488	0.0443	0.0466		0.0443	0.0443
	0.0488	0.0443	0.0466			
	0.0488	0.0443	0.0466	0.0427		0.0427
	0.0488	0.0443	0.0466	0.0443	0.0443	0.0443
mean	0.0488	0.0443	0.0466	0.0435	0.0443	0.0438
vag2	0.0488	0.0427	0.0458			
	0.0473	0.0427	0.0450	0.0473	0.0488	0.0481
	0.0473	0.0473	0.0473	0.0473	0.0488	0.0481
	0.0473	0.0488	0.0481	0.0473	0.0488	0.0481
mean	0.0477	0.0454	0.0465	0.0473	0.0488	0.0481
vag3	0.0504	0.0488	0.0496	0.0504		0.0504
	0.0473	0.0443	0.0458	0.0458	0.0488	0.0473
	0.0488		0.0488			
	0.0488	0.0504	0.0496	0.0519	0.0473	0.0496
mean	0.0488	0.0478	0.0485	0.0494	0.0481	0.0491
vag4	0.0580	0.0412	0.0496	0.0473	0.0473	0.0473
	0.0519	0.0397	0.0458	0.0488	0.0473	0.0481
	0.0519	0.0427	0.0473	0.0473	0.0458	0.0466
	0.0519	0.0412	0.0466	0.0488	0.0473	0.0481
mean	0.0534	0.0412	0.0473	0.0481	0.0469	0.0475

	baseline1	baseline2	avg base	trunk1	trunk2	avg trunk
vag 1	0.0488	0.0443	0.0466	0.0435	0.0443	0.0438
vag 2	0.0477	0.0454	0.0465	0.0473	0.0488	0.0481
vag 3	0.0488	0.0478	0.0485	0.0494	0.0481	0.0491
vag 4	0.0534	0.0412	0.0473	0.0481	0.0469	0.0475
mean	0.0497	0.0447	0.0472	0.0471	0.0470	0.0471
t-test (with avg baseline)				0.8825	0.8509	0.9150

Vagotomy Power Results (from integration of PSD over 0 to 0.1 Hz)

	by region						by region (normalized by percentage change from average baseline)					outliers removed			
	baseline1	baseline2	avg base	trunk1	trunk2	avg trunk	avg base	trunk1	trunk2	avg trunk	t-test	trunk1	trunk2	avg trunk	t-test
fundus	14229	22439	18334	16435	6936	11686	0	-10.3578	-62.1686	-36.2632		-10.3578	-62.1686	-36.2632	
	8100	79914	44007	16911	45665	31288	0	-61.5720	3.7676	-28.9022	0.0807	-61.5720	3.7676	-28.9022	0.0807
	9235	7903	8569	7236	7085	7161	0	-15.5561	-17.3182	-16.4372	0.1278	-15.5561	-17.3182	-16.4372	0.1278
	28281	8105	18193	6040	7709	6875	0	-66.8004	-57.6266	-62.2135	0.0338	-66.8004	-57.6266	-62.2135	0.0338
	14961	29590	22276	11656	16849	14252	0	-38.5716	-33.3365	-35.9540		-38.5716	-33.3365	-35.9540	
	4635	17116	7596	2909	9607	5785	0	14.8650	15.9546	9.6622		14.8650	15.9546	9.6622	
corpus	10725	7541	9133	5346	6624	5985	0	-41.4650	-27.4718	-34.4684		-41.4650	-27.4718	-34.4684	
	9850	67938	38894	15429	39555	27492	0	-60.3306	1.6995	-29.3156	0.0026	-60.3306	1.6995	-29.3156	0.0026
	66933	47107	57020	16412	72821	44617	0	-71.2171	27.7113	-21.7529	0.4828	-71.2171	27.7113	-21.7529	0.4828
	29466	8194	18830	6768	6286	6527	0	-64.0574	-66.6171	-65.3372	0.0291	-64.0574	-66.6171	-65.3372	0.0291
	29244	32695	30969	10989	31322	21155	0	-59.2675	-16.1695	-37.7185		-59.2675	-16.1695	-37.7185	
	13353	14952	10668	2869	15882	9286	0	6.3495	20.2434	9.5693		6.3495	20.2434	9.5693	
p. antrum	9374	14486	11930	4582	3543	4063	0	-61.5926	-70.3018	-65.9472		-61.5926	-70.3018	-65.9472	
	27570	69189	48380	15535	95776	55656	0	-67.8893	97.9681	15.0394	0.6100	-67.8893			0.0047
	10995	12890	11943	72045	7282	39664	0	503.2656	-39.0245	232.1206	0.8409		-39.0245		0.0953
	5881	9292	7587	3531	6007	4769	0	-53.4568	-20.8199	-37.1383	0.6305	-53.4568	-20.8199	-37.1383	0.1735
	13455	26464	19960	23923	28152	26038	0	80.0817	-8.0445	36.0186		-60.9796	-43.3820	-51.5428	
	4824	14283	9529	16269	22555	12904	0	141.0922	36.7850	67.4815		4.1776	14.4494	14.4044	
d. antrum	32761	38473	35617	15077	9835	12456	0	-57.6691	-72.3868	-65.0279		-57.6691	-72.3868	-65.0279	
	31809	64147	47978	14073	34373	24223	0	-70.6678	-28.3567	-49.5123	0.0662	-70.6678	-28.3567	-49.5123	0.0662
	16260	16831	16546	16834	18216	17525	0	1.7437	10.0964	5.9200	0.1409	1.7437	10.0964	5.9200	0.1409
	39443	36081	37762	16583	19686	18135	0	-56.0855	-47.8682	-51.9769	0.0838	-56.0855	-47.8682	-51.9769	0.0838
	30068	38883	34476	15642	20528	18085	0	-45.6697	-34.6288	-40.1493		-45.6697	-34.6288	-40.1493	
	4906	9715	6557	651	5100	2410	0	16.1385	17.4180	15.7292		16.1385	17.4180	15.7292	

* units are the same as in Table 6.2

Table 6.5: Changes in Signal Power With Vagotomy

6.2.1.1 Discussion

Vagotomy removes the direct connection between the brainstem and the enteric nervous system. As well, the minority of direct innervation of the effector cells by the vagus is also removed. The results of vagotomy experiments lead to the conclusion that vagotomy causes a decrease in slow wave amplitude or signal power, and, unlike atropine, no change in dominant frequency.

Although the relationship between intrinsic and extrinsic neurons is still an issue for investigation, it is believed that a majority of vagal neurons only innervate the enteric nervous system, while a minority directly innervate the smooth muscle cells[1,2]. Vagotomy removes the excitatory effect of this minority of cholinergic smooth muscle innervation. The vagal input to the enteric system, however, is a more complex mechanism.

The following is a general hypothesis for the neural control of GEA under normal conditions. The nervous connections to the gastric smooth muscle, both excitatory and inhibitory, provide a GEA mediating stimulus from the enteric nervous system. Under normal conditions, these neural connections deliver the necessary pattern of excitation and inhibition to contribute, along with other generating mechanisms such as interstitial cells of Cajal, to the normal generation of GEA, which results in normal motility. It is hypothesized that extrinsic input to the enteric system, via sympathetic and parasympathetic innervation, as well as intrinsic sensory input, stimulates the enteric system in a particular manner as to elicit the appropriate patterns necessary for normal

generation of GEA. A vagotomy changes the stimulation pattern of enteric input, and thus the elicited pattern of stimulation of the smooth muscle. Very abstractly, the enteric nervous system may be hypothesized to act as a memory system, converting input stimulation from sympathetic, parasympathetic, and local afferent innervation, to different patterns of stimulation of the gastric smooth muscle. Hence, the state of motility in the stomach is altered by alterations in GEA due to different stimulation patterns elicited by neural inputs to the enteric system.

It is very difficult to explain or even hypothesize about the possible underlying mechanisms responsible for the observed response to vagotomy. It is simply observed that this particular change in enteric input, absence of vagal input, results in a stimulation pattern which decreases slow wave amplitude but does not alter its frequency.

6.2.2 Bretylium

Bretylium is classified as an adrenergic nerve blocking agent wich interferes with transmitter release. It is believed to exert a selective anesthetic effect at adrenergic nerve terminals, where it causes the liberation of norepinephrine from nerve terminals with subsequent blocking of release of the transmitter [8]. A major side effect of this drug, however, is hypotension. The major effect of bretylium is to effectively break sympathetic connection with the enteric nervous system.

Bretylium was given intravenously to 2 rats by the standard procedure outlined in appendix B.3. The lack of data prevents statistical significance, however a brief discussion of the obtained results is included.

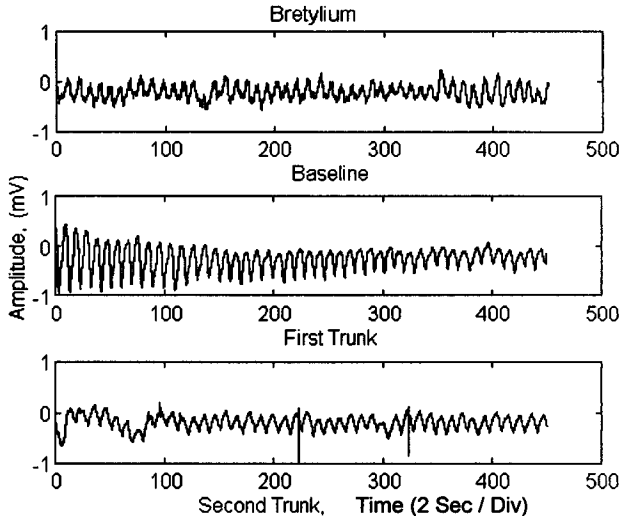

Figure 6.4: Effects of Bretylium on GEA

The IV injection of bretylium seemed to result in two dramatic alterations in recorded GEA. First, the slow wave became much more regular in shape after the injection. Second, the amplitude of the recorded slow wave increased significantly from baseline levels and eventually returned to baseline levels as the effects of the bretylium diminished. Figure 6.4 illustrates these effects.

As with the vagotomy, the breaking of an extrinsic neural connection alters the state of a complex control mechanism. However, it is known that sympathetic gastric innervation inhibits gastric motility. This point is grossly consistent with the results obtained. By injecting bretylium, extrinsic neural input into the enteric nervous system is altered in such a way as to remove inhibitory stimulus on the muscle cells. The removal of these inhibitory factors causes an increase in recorded GEA. The mechanism by which it does this is unknown. It may be possible that neurotransmitter release which opens inhibitory ion channels is reduced, however, many other mechanism may have a role.

6.3 Model

Based on background anatomy, physiology, and known neural pathways, reviewed previously, the GEA neural control system model of Figure 6.5 is hypothesized. Normal GEA generation is hypothesized to occur as follows. The inherent rhythmicity of the interstitial cells of Cajal continually stimulate the gastric muscle cells. This stimulation, in the presence of other appropriate stimulants, periodically raises the muscle cell membrane potential above its threshold, eliciting a depolarization - repolarization wave. This wave propagates very quickly around the circumference in the circular muscle layer due to abundance of coupling, gap junctions. It also propagates slower distally in the longitudinal muscle layer by other mechanisms. This electrical activity differs between regions due to differences in the smooth muscle cell electrical characteristics. Nerves of the autonomic nervous system send signals to the enteric nervous system, both excitatory and inhibitory, and cause the enteric system to elicit appropriate stimulation patterns to control the smooth muscle. This enteric neuron mediation may be directly by alteration of muscle cell membrane potential or by controlling the rhythmic stimulation of the interstitial cells of Cajal, which are known to be highly innervated. Sensory neurons send information back to the enteric nervous system directly, or indirectly through an autonomic neural pathway. This sensory information alters the state of the enteric system in appropriate ways to change GEA according to needs of the gastrointestinal tract. Many neurotransmitters, pathways, and other factors make this control system very complex. In

fact the enteric nervous system is often referred to as the "little brain", responsible for the gastrointestinal tract in much the same way as our brain controls our body.

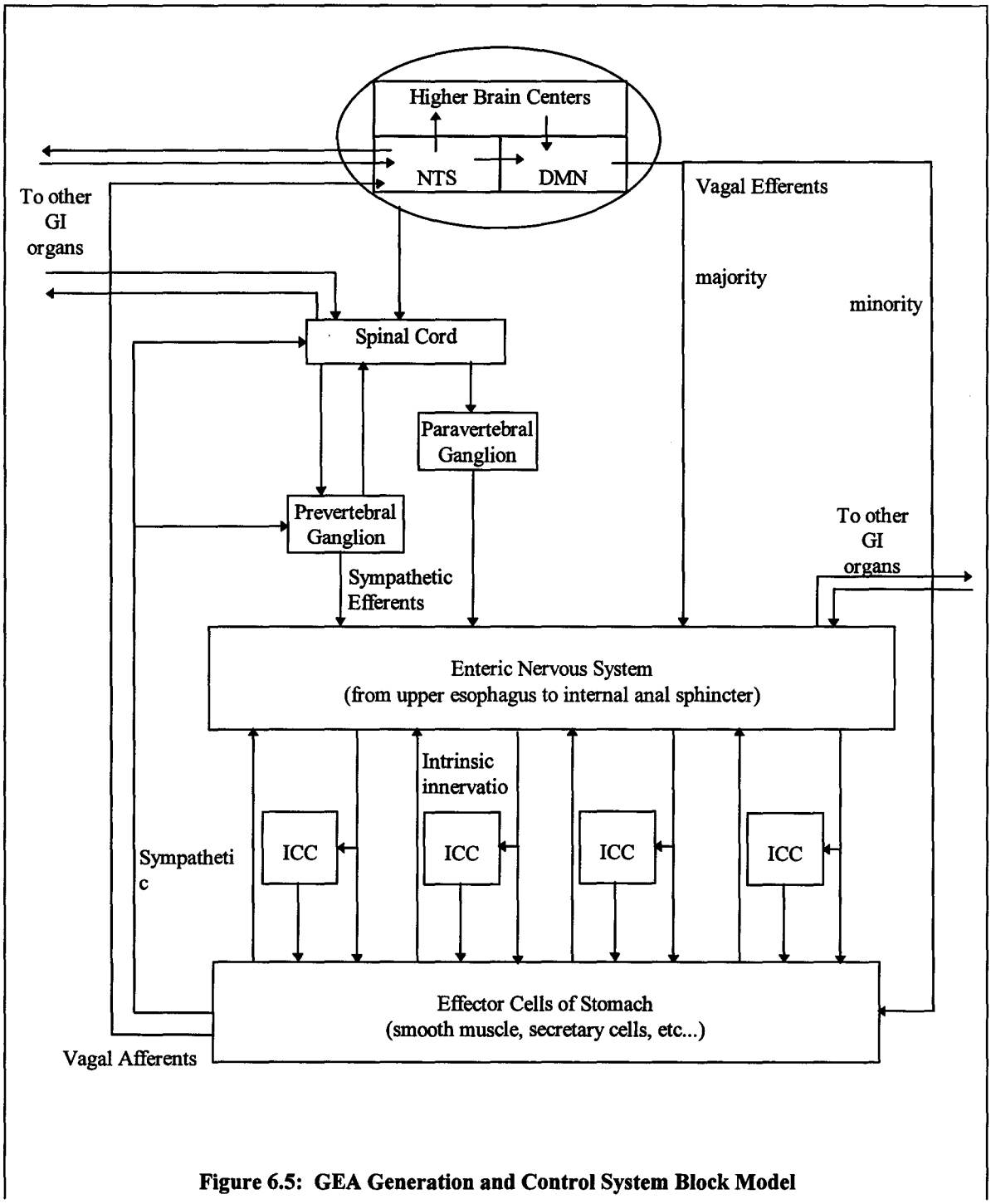

Figure 6.5: GEA Generation and Control System Block Model

6.4 Conclusion

The research tool and methodology developed throughout the course of this project has permitted the investigation of the gastric neural control system. Although only the surface of this investigation has been scratched, the research methodology is in place to investigate each component of this system. Finely tuned experimental procedures, electrode placement techniques, and signal enhancement techniques, have provided a means to examine the results of perturbations in the neural control system. This tool has been applied to several stimuli, including atropine, bretylium, and truncal vagotomy. The results, although open to interpretation, have shown clear responses to these stimuli.

Future work in this area may include the complete system identification. This would involve many different forms of stimulation, changing system input conditions to identify how the system responds. Methods to perform such tasks are well developed aspects of several engineering disciplines and may be applied here. As well, this system could be modeled by a neural network. In fact, since this system is itself a network of neurons, the structure of the neural network model would be based on known structures. Finally, improvements could be made on the quality of the data acquisition system, involving electrode improvements, amplifier improvements, and more complex digital processing algorithms.

Appendix A

Electrogastric Signal Amplifier

A.0 Signal Amplifier Overview

Several electrical properties of electrogastric signals were taken into consideration during the design of the electrogastric signal amplifier. The signal was known to contain a "slow wave" component in the approximate frequency range of 0.02 to 0.16, "spike potentials" thought to be in the range of 1 to 10 Hz, and very slow DC shifts. Therefore, the bandwidth of the amplifier was set at 0.01 to 20 Hz and a DC offset was to added to compensate for polarization of electrodes, motion, and very slow DC shifts. This limited bandwidth is wide enough to encompass all desired components while at the same time eliminating high frequency noise, 60 Hz line pickup, and EMG artifact. In order to make the amplifier flexible enough to handle both serosal, 0.5 mV to 10 mV, and surface, 10 μV to 500 μV, recordings, the gain was designed to be adjustable to several preset gains. The overall amplifier gain was split up into three sections, the differential pre-amplifier, DC offset incorporated gain, and the switchable gain stage. Figure A.0 is a block diagram of the amplifier, as well as a schematic representation of the amplifier front end.

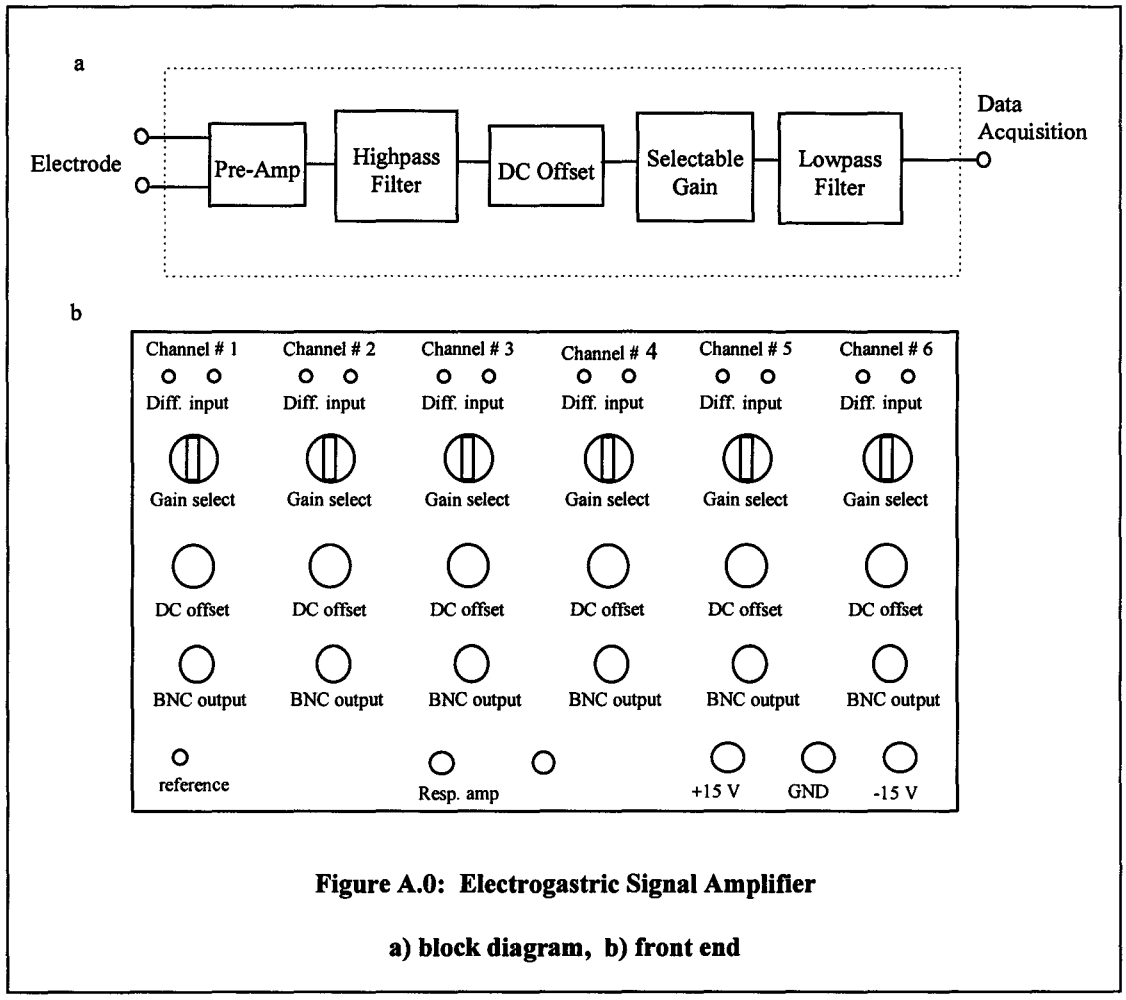

Figure A.0: Electrogastric Signal Amplifier

a) block diagram, b) front end

A.1 Pre - Amplifier

The pre-amplifier was designed using a monolithic instrumentation amplifier manufactured by Analog Devices [18], the AD620bn. It was resistor strapped to implement a gain of approximately 10. The resistor was chosen according to the supplied gain equation:

$G = 1+49.4k / R_G$. This instrumentation amplifier is based on the classic three op-amp design the specifics of which may be examined in the accompanying data sheets [18].

A.2 High Pass Filter

The butterworth response was chosen due to its maximally flat passband response. The phase response is irrelevant since phase delays will be calculated between recordings recorded from identical amplifier channels. Therefore, any phase non-linearities will be present in both signals and will not be a factor in the estimation of phase delay. A second order filter with cut-off frequency of 0.01 Hz was determined to be sufficient for implementation of the low frequency cut-off. A unity - gain Sallen - Key highpass filter was implemented, having the following transfer function:

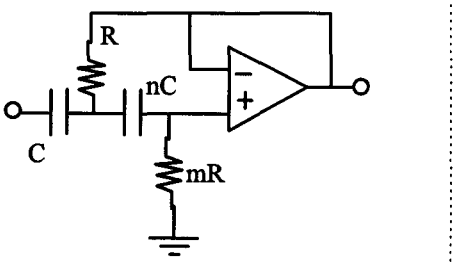

Figure A.1: 2nd Order Butterworth Highpass Filter

$$H = \frac{-(f/f_o)^2}{1-(f/f_o)^2+(j/Q)(f/f_o)}.$$

where: $f_o = \frac{1}{2\pi\sqrt{(mn)}RC}.$

and $Q = \frac{\sqrt{(mn)}.}{n+1}$

Parameters were chosen to fit values to standard component values for best accuracy with m = 2 and n = 1 for a butterworth response.

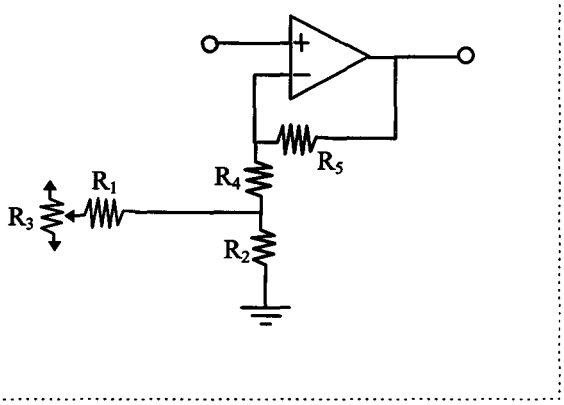

Figure A.2: DC Offset Adjust

A.3 DC Offset

The DC offset, shown in Figure A.2, was designed to introduce a gain of 20 and have a DC adjust range of +/- 0.3 V. Range and gain are determined by the following relations:

Range = +/- V (R_2 / R_1)

Gain = 1 + R_5 / (R_4 + R_2).

It was also determined that a single turn potentiometer would be used for ease of adjustment.

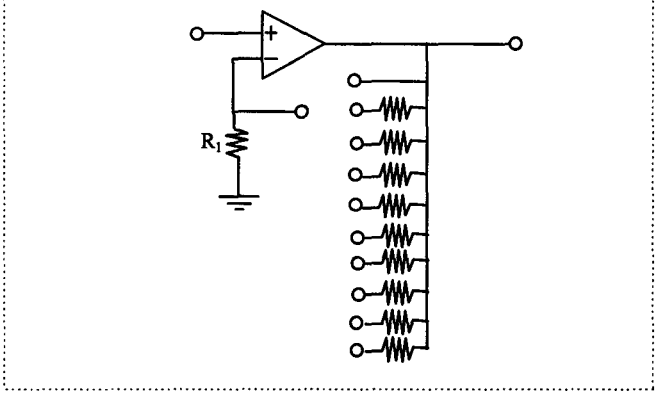

Figure A.3: Selectable Gain

A.4 Selectable Gain

The overall system gain up to this stage is 200 times. The gain of this stage was designed to give the most desirable overall amplifier gains to be appropriate for amplification of both serosal and surface gastric signals. The gains chosen were 1, 2, 5, 10, 30, 75, 150, 300, and 500, giving an overall amplifier gain range of 200 to 100 000.

A.5 Lowpass Filter

It was decided that a butterworth response would be used as well for the lowpass filter, however, a sharper roll - off was required to ensure rejection of low frequency electromyographic interference. For this reason, a fourth order butterworth lowpass filter was implemented using two cascaded second order unity - gain Sallen - Key implementations, in the appropriate combination. From tables in (19) the following

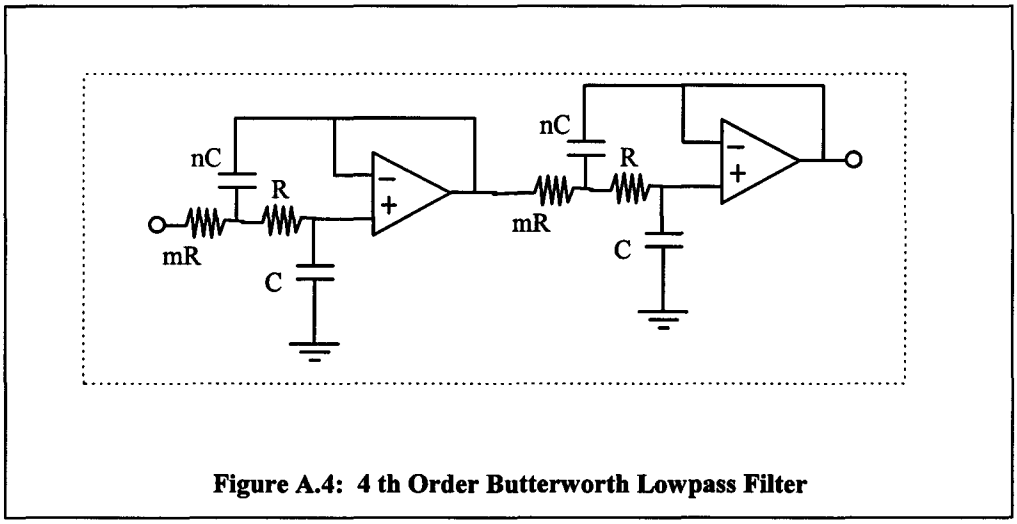

Figure A.4: 4 th Order Butterworth Lowpass Filter

parameters were determined to provide a butterworth response: $Q_1 = 0.541$ and $Q_2 = 1.306$. The transfer function of this filter is:

$$H = \frac{1}{1-(f/f_o)^2+(j/Q)(f/f_o)}. \quad \text{where: } f_o = \frac{1}{2\pi\sqrt{(mn)}RC}. \quad \text{and: } Q = \frac{\sqrt{(mn)}.}{m+1}$$

For a butterworth response the parameter values were chosen with m = 1 and n = 2.

Appendix B

Standard Procedures

B.0 Effect of Accumulated Atropine Dose on Baseline Electrogastric Activity

Objective:

The objective of this study is to determine the change in electrogastric activity in rats associated with blocking of cholinergic nerve pathways by an accumulated dosage of atropine. Since atropine is a cholinergic muscurinic receptor antagonist, it blocks cholinergic nerve connection to the stomach. This change should be indicative of a change in autonomic regulation of the electrical activity of the stomach. By determining this effect we will uncover one part of the neural control system regulating gastric electrical activity.

Apparatus:

anesthetic (90 mg/kg ketamine & 20 mg/kg xylazine)

surgical tools (scissors, scalpel, forceps)

syringe, needle, .1 CC

gauze

clippers

stainless steel wire electrodes

electrode connection wires and harness

signal amplifier

computer and data acquisition equipment

rat

Procedure:

1. obtain rat from CAF and weigh
2. prepare anesthetic needle, determining appropriate dose from weight and chart posted in lab
3. inject anesthetic intramuscularly and wait until animal is at appropriate level (determined by toe - pinch, approximately 15 - 30 minutes)
4. while waiting, prepare surgical tools, heating pad, computer, and other equipment
5. at appropriate time, shave animal from xiphoid to pubic area
6. move animal to heating pad, and cut along the midline with the scalpel, taking care to only incise the skin
7. lift muscle layer with forceps and cut small incision with the scissors, use scissors to carefully free muscle from underlying tissue, use scissors, cutting along the midline, to expose the peritoneal cavity
8. use locking forceps to hold cavity open
9. with fingers, gently lift liver and carefully expose stomach so that it is visible and exposed enough to attach electrodes to all regions

10. attach electrodes (stainless steel wire electrodes) to appropriate locations, indicated below, including reference electrode, placed slightly above muscle of right hind leg, and ground electrode, placed slightly above muscle of left hind leg (25 gauge needles).

Electrode Placement

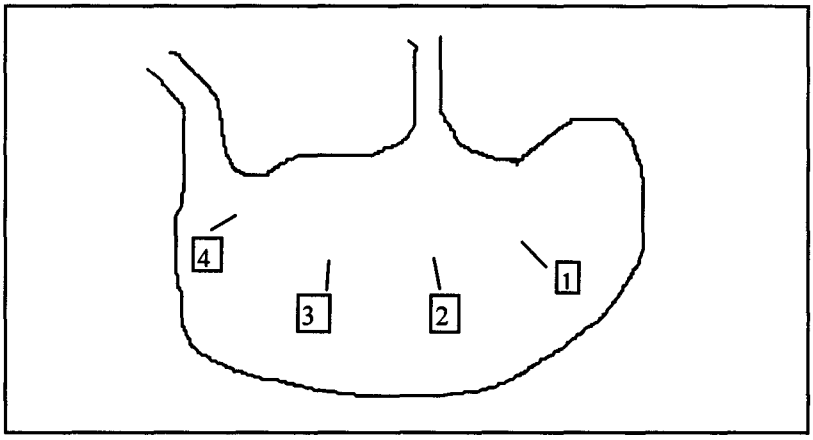

11. wait 5 minutes after stable signals are seen on all electrodes
12. record for 20 minutes (baseline)
13. wait 10 minutes
14. inject appropriate amount of atropine solution to give first dose of 3.75 mg/kg
15. wait 10 minutes, prepare atropine needle
16. record for 20 minutes (first dose)
17. inject appropriate amount of atropine solution to give second dose of 3.75 mg/kg (total accumulated dose of approximately 7.5 mg/kg)
18. wait 10 minutes, prepare atropine needle

19. record for 20 minutes (second dose)

20. inject appropriate amount of atropine solution to give third dose of 7.5 mg/kg (total accumulated dose of approximately 15 mg/kg)

21. wait 10 minutes, prepare atropine needle

22. record for 20 minutes (third dose)

23. euthanise animal via cardiac puncture with urethane and air

24. clean up lab and transfer recordings to processing computer

B.1 Effect of Vagotomy on Baseline Electrogastric Activity

Objective:

The objective of this study is to determine the change in electrogastric activity in rats associated with a complete blockade of preganglionic parasympathetic innervation (vagus).

Apparatus:

anesthetic (90 mg/kg ketamine & 20 mg/kg xylazine)

surgical tools (scissors, scalpel, forceps)

syringe, needle

gauze

clippers

stainless steel wire electrodes

electrode connection wires and harness

signal amplifier

computer and data acquisition equipment

rat

suture

microscope

Procedure:

1. obtain rat from CAF and weigh
2. prepare anesthetic needle, determining appropriate dose from weight and chart posted in lab
3. inject anesthetic intramuscularly and wait until animal is at appropriate level (determined by toe - pinch, approximately 15 - 30 minutes)
4. while waiting, prepare surgical tools, heating pad, computer, and other necessary equipment
5. at appropriate time, shave animal from xiphoid to pubic area
6. move animal to heating pad, and cut along the midline with the scalpel, taking care to only incise the skin
7. lift muscle layer with forceps and cut small incision with the scissors, use scissors to carefully free muscle from underlying tissue, use scissors, cutting along the midline, to expose the peritoneal cavity
8. use locking forceps to hold cavity open

9. with fingers, gently lift liver and carefully expose stomach so that it is visible and exposed enough to attach electrodes to all regions
10. locate anterior and posterior vagus nerve trunks with microscope. Tie suture around each vagus nerve.
11. attach electrodes (stainless steel wire electrodes) to appropriate locations, as in atropine experiment, including reference electrode, placed slightly above muscle of right hind leg, and ground electrode, placed slightly above muscle of left hind leg (25 gauge needles).
12. wait 5 minutes after stable signals are seen on all electrodes
13. record for 20 minutes (baseline recording)
14. wait 10 minutes
15. record for 20 minutes (2^{nd} baseline recording)
16. tighten suture knot around one vagus nerve to block axonal flow
17. wait 10 minutes for signal stabilization
18. record for 20 minutes (1^{st} vagotomy recording)
19. wait 10 minutes
20. tighten knot around second vagus trunk
21. record for 20 minutes (2^{nd} vagotomy recording)
22. euthanise animal via cardiac puncture with urethane and air
23. clean up lab and transfer recordings to processing computer

B.2 Effect of Bretylium on Baseline Electrogastric Activity

Objective:

The objective of this study is to determine the change in electrogastric activity in rats associated with the temporary blockade of inhibitory sympathetic nerve fibers by the intravenous injection of bretylium.

Apparatus:

anesthetic (90 mg/kg ketamine & 20 mg/kg xylazine)

surgical tools (scissors, scalpel, forceps)

syringe, needle

gauze

clippers

stainless steel wire electrodes

electrode connection wires and harness

signal amplifier

computer and data acquisition equipment

rat

suture

Procedure:

1. obtain rat from CAF and weigh

2. prepare anesthetic needle, determining appropriate dose from weight and chart posted in lab
3. inject anesthetic intramuscularly and wait until animal is at appropriate level (determined by toe - pinch, approximately 15 - 30 minutes)
4. while waiting, prepare surgical tools, heating pad, computer, and other necessary equipment
5. at appropriate time, shave animal from xiphoid to pubic area
6. move animal to heating pad, and cut along the midline with the scalpel, taking care to only incise the skin
7. lift muscle layer with forceps and cut small incision with the scissors, use scissors to carefully free muscle from underlying tissue, use scissors, cutting along the midline, to expose the peritoneal cavity
8. use locking forceps to hold cavity open
9. with fingers, gently lift liver and carefully expose stomach so that it is visible and exposed enough to attach electrodes to all regions
10. attach electrodes (stainless steel wire electrodes) to appropriate locations, as in atropine experiment, including reference electrode, placed slightly above muscle of right hind leg, and ground electrode, placed slightly above muscle of left hind leg (25 gauge needles).
11. wait 5 minutes after stable signals are seen on all electrodes
12. record for 20 minutes (baseline recording)

13. wait 10 minutes

14. record for 20 minutes (2^{nd} baseline recording)

15. give IV injection of bretylium (15mg / kg dose)

16. immediately record for 20 minutes (1^{st} vagotomy recording)

17. wait 10 minutes

18. record for another 20 minutes (2^{nd} vagotomy recording)

19. euthanise animal via cardiac puncture with urethane and air

20. clean up lab and transfer recordings to processing computer

Bibliography

1 Tadataka Yamada. *Textbook of Gastroenterology: Volume 1.* J. B. Lippincott Company, Philadelphia, 1991.

2 Arthur C. Guyton and John E. Hall. *Textbook of Medical Physiology, 9th Edition.* W. B. Saunders Company, Philadelphia, 1996.

3 Jan D. Huizinga. *Interstitial Cells of Cajal as Pacemaker Cells of the Gut.* Academic Press Limited, 1996.

4 Martin P. Mintchev and Kenneth L. Bows. Electrical Phenomena in the Human Stomach. *www.ee.ualberta.ca/~mintchev/www.html*, 1995-1996.

5 Hak W. Tam and John G. Webster. Minimizing Electrode Motion Artifact by Skin Abrasion. *IEEE Trans. Bio. Med.*, (24): 134-139, March 1977.

6 A. J. P. M. Smout, E. J. Van Der Schee and J. L. Grashuis. What is Measured in Electrogastrography?. *Digestive Diseases and Science*, (25): 179-187, March 1980.

7 J. Chen, R. W. McCallum and R. Richards. Frequency Components of The Electrogastrogram And Their Correlations With Gastrointestinal Contractions in Humans. *Med. & Bio. Eng. & Comput.*, (31): 57-60, January 1993.

8 Charles H. Hockman. *Essentials of Autonomic Function.* Charles C Thomas, Springfied.

9 Arnon Cohen. *Biomedical Signal Processing Volume 1 Time and Frequency Domains Analysis* CRC Press Inc., Boca Raton, Florida, 1986.

10 Samuel D. Stearns and Don R. Hush. *Digital Signal Analysis* Prentice-Hall Inc., Englewood, New Jersey, 1990.

11 Boaz Porat. *Digital Processing of Random Signals Theory & Methods.* Prentice-Hall Inc., Englewood Cliffs, New Jersey, 1994.

12 Jiande Z. Chen and Richard W McCallum. Acquisition & Analysis of Electrogastric Data. *Electrogastrography. Principles & Applications*, Raven Press, New York, NY, 1994.

13 Jiande Z. Chen and Richard W McCallum. Electrogastrography· Measurement, Analysis and Prospective Applications. *Med. & Bio. Eng. & Comput.,* (29): 339 - 350, 1991

14 Steven M. Kay *Modern Spectral Estimation. Theory & Application.* Prentice - Hall Inc., Englewood Cliffs, NJ, 1988.

15 Paul A. Taylor *Process Identification Notes.* McMaster University Press, 1993.

16 Mary F Otterson and Michael G. Sarr Normal Physiology of Small Intestinal Motility *Surgical Clinics of North America*, 6(73): 1173 - 1191, Dec. 1993.

17 Michael E. Zenilman. Origin and Control of Gastrointestinal Motility *Surgical Clinics of North America,* 6(73): 1081 - 1099, Dec. 1993.

18 Analog Devices, Data Book

19 S. Franco. *Design with Operational Amplifiers and Analog Integrated Circuits.* McGraw - Hill Inc., 1988.

20 Jiande Z. Chen, J. Vandwalle and W. Sansen. Adaptive Method for Cancellation of Respiratory Artefact in Electrogastric Measurements. *Med. & Biol. Eng. & Comput.*, (27): 57-63, 1989.

21 Hak W. Tam and John G. Webster. Minimizing Electrode Motion Artifact by Skin Abrasion. *IEEE Trans. Biomed. Eng.*, (24): 134-139, 1977.

22 E. J. Van Der Schee and J. L. Grashuis. Running Spectrum Analysis as an Aid in The Representation and Interpretation of Electrogastrographic Signals. *Med. & Biol. Eng. & Comput.*, (25): 57-62.

23 D. A. Linkens and S. P. Datardina. Estimation of Frequencies of Gastrointestinal Electrical Rhythms Using Autoregressive Modeling. *Med. & Biol. Eng. & Comput.*, (16): 262-268, 1978.

24 Deutsch A. Welkowitz. *Biomedical Instruments (Theory and Design)*. 1992.

25 Thomas P. Krauss, Loren Shure and John N. Little. *Signal Processing Toolbox User's Guide*. The MathWorks Inc., Natick, Mass., 1995.

26 AT / MCA Codas and Windaq User's Manual, DataQ Instruments, Inc., Akron, Ohio

27 M. T. Silvia. Time Delay Estimation. *Handbook of Digital Signal Processing*, Academic Press Inc., 1987

28 Y. J. Kingma. The Electrogastrogram and Its Analysis. *Critical Reviews in Biomedical Engineering*, (17): 105 - 132, 1989.